國 立 交 通 大 學

光電工程研究所

博士論文

錨定能對液晶盒動態響應的影響

Effects of Anchoring Energy on the Dynamic Response of Liquid Crystal Cells

研究生: 徐芝珊

指導教授: 王淑霞 教授

梁寶芝 教授

中華民國 九十四 年 六 月

錨定能對液晶盒動態響應的影響

Effects of Anchoring Energy on the Dynamic Response of Liquid Crystal Cells

研究生：徐芝珊　　Student: Jy-Shan Hsu

指導教授：王淑霞　　Advisor: Prof. Shu-Hsia Chen

梁寶芝　　Prof. Bau-Jy Liang

國立交通大學光電工程研究所

博士論文

A Dissertation

Submitted to Institute of Electro-Optical Engineering

National Chiao Tung University

in Partial Fulfillment of the Requirements

for the Degree of Doctor of Philosophy

in Electro-Optical Engineering

June 2005

Hsinchu, Taiwan

中華名國九十四年六月

錨定能對液晶盒動態響應的影響

研究生：徐芝珊　　指導教授：王淑霞教授

梁寶芝教授

國立交通大學光電工程研究所

摘　要

液晶的動態行為在液晶元件光學反應的研究中，是一個非常基本也非常重要的課題。液晶的動態特性不僅與液晶的材料性質有關，更與液晶排列方式有著密不可分的關係。液晶的排列方式會被邊界條件所左右，其邊界條件可用錨定能密度來表示，錨定能密度則可由 easy axis 的位置與錨定能係數來決定。此外，在向列型液晶中，其指向矢的轉動與流動是互相耦合在一起的。例如：液晶指向矢的非均勻轉動會造成流動的發生，而流動亦會干擾指向矢的轉動，此效應可以在扭轉型液晶盒的光學跳躍現象與雙穩態驅動機制中發現。

本論文中，我們先研究錨定能密度並用雙穩態液晶盒為例，來探討其對流動效應的影響。在錨定能密度中，預傾角是 easy axis 在極角方向的傾角。我們推導出液晶盒在外加電壓下，預傾角與相位延遲的關係，解決了測量垂直排列反射式液晶盒預傾角的問題。在測量錨定能係數時，我們發現若外加電壓使得邊界上的指向矢偏離 easy axis 變大，只考慮一項的錨定能密度函數是不合適的，此時必須加進高次項來修正。我們用包含高次項的錨定能密度模型，測量並分析二個水平排列與三個垂直排列的液晶盒所具有的錨定能係數。

此外，我們以水平配向，一邊界為強錨定，另一邊界為弱錨定的雙穩態向列型液晶盒（BiNem）為例，研究在不同脈衝波的作用下，液晶盒光學表現不同的原因與機制。我們發現其弱邊界上的指向矢，在脈衝波作用結束時的位置，會影響後來的液晶動態行為。最後，我們設計並做出一種新的雙穩態液晶顯示模態（BHN）的液晶盒，藉由液晶的流動效應與雙頻液晶的特性，構成轉換機制。在實驗上，其切換電壓僅需為 5 V 即可達成穩態間的轉換。

Effects of Anchoring Energy on the Dynamic Response of Liquid Crystal Cells

Student: Jy-Shan Hsu Advisors: Prof. Shu-Hsia Chen
Prof. Bau-Jy Liang

Institute of Electro-Optical Engineering
National Chiao Tung University

Abstract

Consider as an important subject for the study of the electro-optical response in the liquid crystal (LC) device, the dynamic behaviors of liquid crystals are not only related to the intrinsic properties of the LC material itself but also to the spatial orientation of the LC directors. The arrangement of the directors in a cell is controlled by the boundary conditions, which can be described by the anchoring energy density determined by the position of the easy axis and the coefficients of the anchoring energy density. Moreover, there is a coupling between the translational motion and the rotational motion of the nematic LC directors. For example, the non-uniform rotations of LC directors induce the shear flow of the LC director; conversely, the shear flow disturbs the orientation of the LC directors. The shear flow effect can be observed in the optical bounce of twisted nematic cells and some of the switching mechanisms of bistable devices.

In this research, we first studied the anchoring energy density and than used two bistable cells as examples to investigate the impact of the shear flow effect. Within the anchoring energy density, the pretilt angle is the tilt angle of the easy axis in the polar direction. We derived the relationship between the pretilt angle and the phase retardation as a function of applied electric field and solved the problem of obtaining the pretilt angle

of a non-twisted, vertical aligned reflective cell. When measuring the anchoring energy coefficients, we found the higher order terms of the anchoring energy density cannot be negligible when the applied voltage becomes large. By using the anchoring energy density with one higher order term, we measured the anchoring energy coefficients of two homogeneous cells and three homeotropic cells.

Furthermore, we investigated the optical response of Bistable nematic (BiNem, a homogeneous aligned cell with one weak anchoring substrate and one hard anchoring substrate) cell by applying voltage pulses with various durations. We found that the position of the weak-boundary director at the end of the pulse has a crucial impact on the relaxation behaviors. Finally, we designed and demonstrated a novel bistable mode, namely, the bistable chiral-tilted homeotropic nematic (BHN) LC device. The switching mechanism is achieved by the shear flow effect and the anisotropic properties of a dual frequency liquid crystal. The experimental switching voltage of the device is only 5 V.

致謝

首先感謝我最親愛的父母親： 徐元錫先生及 朱鏡如女士，謝謝他們給予我最大的支持與鼓勵，沒有他們就沒有今天的我。感謝我的公公與婆婆： 黃金玉先生及 黃胡火珠女士的照顧，細心地呵護黃潔和宇冬，讓我無後顧之憂的完成博士學程。此外也要感謝大姊芝倫、二姊芝敏、妹妹夢蘭、大伯文淦、大嫂美雲、大姑秀梅與小姑錦鈴的支持與關心。

特別感謝指導教授 王淑霞老師在學術研究與為人處事上的諄諄教誨，使我在知識與生活上受益良多。指導教授 梁寶芝老師在心靈與生活上的引領，耐心的與我討論研究上的盲點。兩位指導老師使我順利地以嚴謹而且踏實步伐完成此研究及論文。

感謝學長陳立宜博士、楊秋蓮博士與謝志勇博士在理論模擬方面的幫助。感謝俊雄、范姜、怡安帶著我一同準備資格考，那一段一起唸書，討論與打 AOC 以紓解壓力的日子，令人難忘。感謝美琪、品發、家榮陪我一起做實驗，並還幫我收實驗數據，一起討論與分析實驗上所碰到的問題。

感謝孩子們黃潔和宇冬，他們的支持與笑容一直是我心中最大的快樂與支柱。

感謝實驗室的學長姐及學弟妹: 秋蓮、志勇、阿寬、俊雄、范姜、怡安、揚宜、彥廷、信全、乾煌、梓傑、佳成、惠雯、庭瑞、朝旭、英豪、舒展、德源、建宏、世郁、品發、美琪、家榮、庭毅、瑞傑陪我一起走過酸甜苦辣的博士班生活，我們在實驗室的互動為平淡的生活帶來不少的樂趣與歡笑。最後這年，更要感謝范姜、庭毅、瑞傑一起分擔實驗室的工作，並能相互扶持一同畢業。

僅以此論文獻給我最親愛的父母、公婆、孩子們、以及所有關心我和幫助過我的人，謝謝你們。

徐芝珊

新竹交通大學 2005 年 5 月

Contents

List of Figures

List of Tables

List of Symbols

$\vec{D}$	*applied displacement*
$\vec{E}$	*applied electrical field*
F_{total}	*total free energy of the cell*
G_i	*external director body force per unit volume*
V	*applied voltage*
V_{th}	*threshold voltage*
d	*cell gap*
f_{bulk}	*Frank free energy density*
f_{elec}	*electric free energy density*
f_i	*fluid body force per unit volume in i direction*
f_s	*surface free energy density or anchoring energy density*
f_{total}	*total free energy per unit area*
g_i	*intrinsic director body force per unit volume in the i direction*
g_i^0	*static (elastic) part of intrinsic director body force per unit volume in the i direction*
g'_i	*hydrodynamic (viscous) part of intrinsic director body force per unit volume in the i direction*
k_{11}	*splay elastic constant*
k_{22}	*twist elastic constant*
k_{33}	*bend elastic constant*
$\vec{n}$	*director orientation*
n_e	*extraordinary refraction index of liquid crystal*
n_o	*ordinary refraction index of liquid crystal*
q_0	*$q_0=2\pi/p$, p: pitch of colesteric structure*
t_{ji}	*fluid stress tensor*
t_{ji}^0	*elastic part of fluid stress tensor*

t'_{ji} *hydrodynamic part of fluid stress tensor*

v_i *fluid flow velocity*

$\Delta\varepsilon$ *dielectric anisotropy of liquid crystal*

Δn *refractive anisotropy of liquid crystal*

Γ, δ *phase retardation*

α *tilt angle of director*

α_0 *pretilt angle*

α_s *tilt angle of surface director*

$\alpha_1 \sim \alpha_6$ *Leslie viscosity coefficients*

$\varepsilon_{//}$ *dielectric constant parallel to the director of liquid crystal*

$\varepsilon_{\perp}$ *dielectric constant perpendicular to the director of the liquid crystal*

ϕ *azimuthal angle of director*

γ *Largrange multiplier*

γ_1 *rotational viscosity coefficient,* $\gamma_1 = \alpha_3 - \alpha_2$

γ_2 *viscosity coefficient,* $\gamma_2 = \alpha_6 - \alpha_5$

$\eta_1 \sim \eta_3$ *shear viscosity coefficients*

λ *wavelength of light*

π_{ji} *director surface stress tensor*

θ *polar angle of director*

ρ *mass density of fluid*

ρ_1 *moment of inertia*

τ_i *viscous torque*

τ_E *electric torque*

Chapter 1

Introduction

The electro-optical characteristic of a liquid crystal (LC) cell is determined by the bulk behaviors of the molecules. The configuration of LC molecules is, in turn, determined by the arrangement of the LC molecules on the boundary which is controlled by the alignment layer. There are several parameters used to describe the properties of the interface between the LC and alignment layer, such as the coordinates of the easy axis as well as the anchoring energy coefficients. The former describe the minimum position of the interfacial surface free energy and the later determine the abilities of the LC molecules to deviate from the easy axis.

On the other hand, in order to improve the performance of the liquid crystal display (LCD), the dynamic behaviors of the LC molecules need to be investigated. The shear flow effect, which is sometimes ignored in the LCD design, can affect the optical response of the LCD. In this chapter, we briefly describe these effects with different boundary conditions.

1.1 The meaning of the anchoring energy

The interaction between the LC molecules and the alignment layer is subtle. From the macroscopic view, we adopt the surface free energy density (anchoring energy density) to describe the characteristic interface interaction. Without any external force, the LC molecules on the boundary are aligned in the easy axis, as shown in Figure 1.1 (a), which orient in the minimum state of the surface free energy density. When there are external forces acting on the LC molecules, the boundary director deviates from the easy axis, which is shown in Figure 1.1 (b).

To describe the surface effect, Rapini and Papoular[1] introduced a simple phenomenological expression for the interfacial surface free energy per unit area, f_s, which describes the interaction between the nematic LC director and the substrate of homeotropic

anchoring: $f_s = \frac{1}{2} W \sin^2(\theta)$, where θ is the polar angle of the director and W is the anchoring energy coefficient. The larger the W, the harder the director can be deviated from easy axis, which is the strong anchoring boundary condition. Small W means weak anchoring boundary condition. After Rapini-Papoular's (R-P) work, many attempts have been made to generalize the RP model in order to describe the planar and tilt anchoring properties. The anchoring energy coefficients of a planar surface direction are the azimuthal anchoring energy coefficient W_ϕ, which is related to the deviations from the easy axis in the azimuthal direction, and the polar anchoring coefficient W_θ, which is corresponding to the deviations from the easy axis in the polar direction.

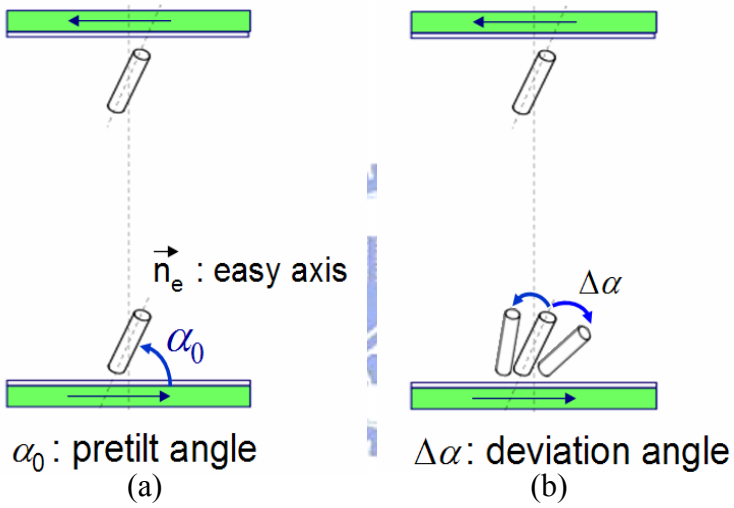

Figure 1.1 Sketch of geometry for the easy axis and the deviation angle.

1.2 The dynamic response of liquid crystal cell

The dynamical behavior [2,3] of liquid crystal displays (LCDs) is not only related to the LC materials but also to the boundary parameters. Due to the complication of the dynamical problem which is associated with five nonlinear coupling equations of the director and flow velocity, it is difficult to deduce the analytic form. Usually, the flow effect of liquid crystals and the boundary conditions are simplified by considering only the rotational viscosity and rigid boundary condition, respectively. Under the pure rotational model with rigid boundaries, only a time constant is used to characterize the response time of the LC devices, which is derived through the equation of motion of the director balanced between the

rotational viscous, elastic and electric torques. However, without the consideration of shear flow effect and the boundary condition carefully, the dynamical behavior of the LC devices can not be predicted accurately.

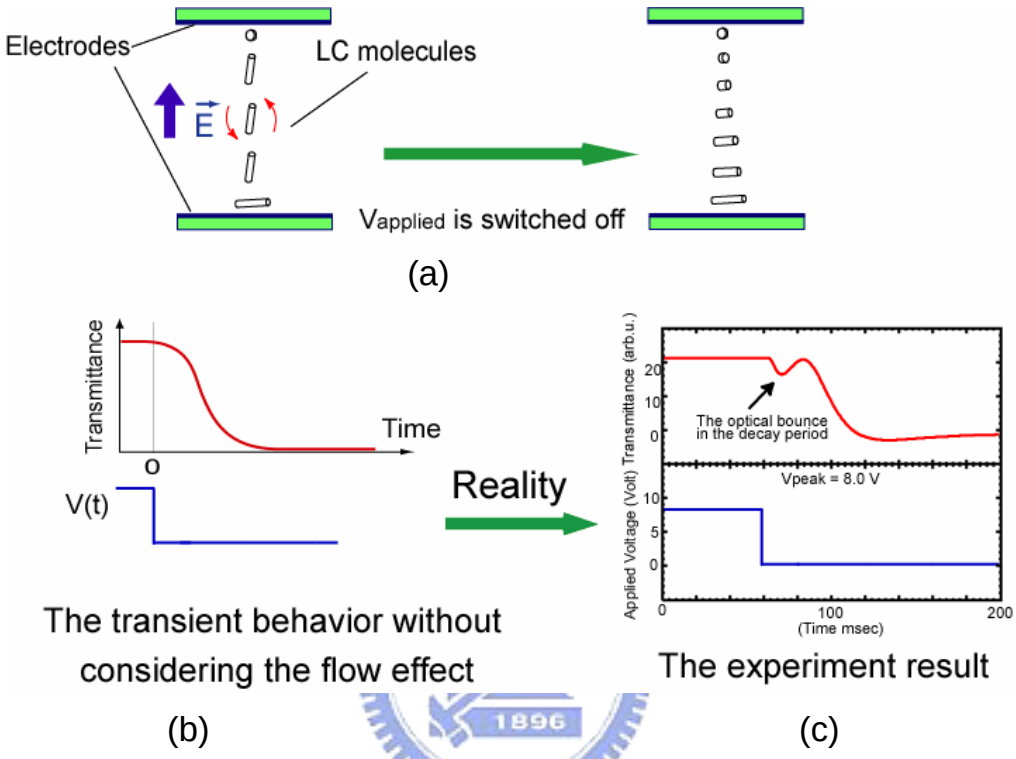

Figure 1.2 (a) The director configuration of a twisted nematic cell under normally black mode before and after the switching off process. (b) The calculated transient intensity without considering the flow effect. (c) The optical bounce can be found in the transient intensity after turning off the applied voltage in the experimental data.

1.2.1 For cells with strong anchoring

Usually the LC boundary directors are regarded as they are rigidly anchored on the substrates, although, it is never true for the boundary directors. It is a good approximation for the rubbed polyimide (PI) alignment layers. From the reported literature, the measured polar and azimuthal anchoring energy coefficients of the rubbed PI are around 10^{-3} J/m^2 and 10^{-4} J/m^2, respectively, which makes the behaviors of the LC directors closed to that of the rigid boundary condition.

Figure 1.2 shows a twisted nematic (TN) LC cell being switched off from a high field.

The transient behaviors, which do not include the shear flow effect, are different from the experimental results. Figures 1.2 (b) and (c) illustrate an optical bounce in the decay process of the experimental result while there is not in the simulation when the shear flow effect is not included. The dynamical behaviors, which exist in the TN-mode LC device have been studied more than 20 years since van Doorn [4] and Berreman [5] independently showed that the importance of hydrodynamic flow in the transient behavior of liquid crystals. The optical bounce in the decay process originates from the flow-induced tipped-over and reverse twist effect of liquid crystals. In addition to the decay process, the shear flow effect influences the director orientation in the rising process. Though, there are no significant effects on the optical response.

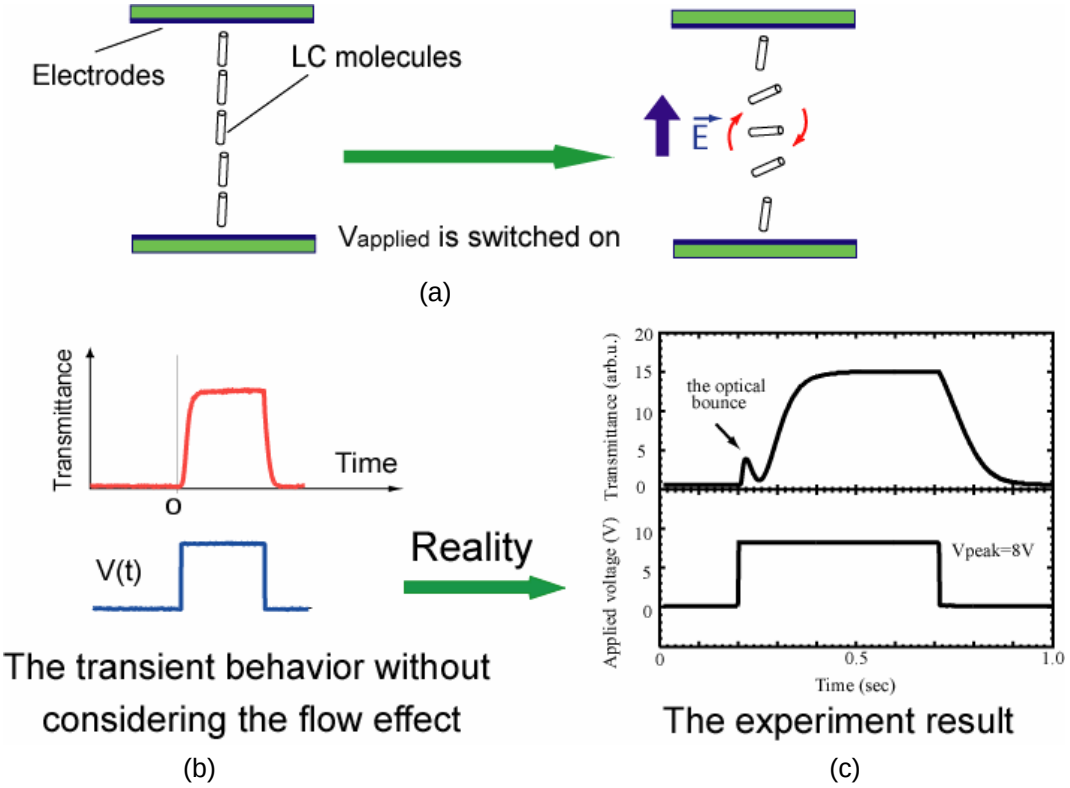

Figure 1.3 (a) The director configuration of a quasi-homeotropic nematic cell before and after the switching on process. (b) The calculated transient intensity without considering the flow effect. (c) The optical bounce can be found in the transient intensity after turning on the applied voltage in the experimental data.

The shear flow effect can also be observed in the transient behavior when a quasi-homeotropic cell is switched to a high field [6-12]. Figure 1.3 (a) shows the director configuration of a quasi-homeotropic nematic LC cell being switched on to a high field. Figure 1.3 (b) shows when the flow effect is not included, the simulated optical response of

the switch on process rises smoothly. However, Figure 1.3 (c) shows a bump in the experimental result. The detailed switching mechanisms have been studied by Dr. Chen [6-9] and Dr. Hsieh [10-12] of our group and the reasons causes of the optical bounce are the shear flow and the asymmetry of the boundary [11].

These two examples illustrate the varied results of the shear flow effect on the transient behaviors of TN and quasi-homeotropic cells with hard anchoring boundary. Since the alignments of the boundaries in the cells are different, the configurations of the directors are different; the effects of the shear flow are distinct and need to be studied carefully.

1.2.2 For cells with weak anchoring

In addition to the rubbed PI, there are many ways to align LC molecules on the substrates, e.g. SiO_x sputtering, photo-alignment, atomic-beam alignment, atomic force microscope scan method. Since the interfacial anchoring properties of these alignment methods vary from hard to weak, one should not regard the boundary directors as they are rigidly anchored on the substrates. Recently, the photo-alignment materials are getting more stable and popular in the application of LCDs. For better understanding the behaviors of the displays, we should include the surface free energy density in the modeling of LCD.

In general, when a small field is applied to a LC cell, the shear flow effect is small and can be ignored. The directors simply rotate toward the direction of the field. Since the directors on the boundaries can be rotated easier for the weaker anchored directors, the cell moves to the final on state faster. Therefore, the response time of weakly anchored boundary directors is less than that of the hard anchored boundary directors. However, when the field is tuned off, the final state is determined by the relaxation process. The weakly anchored directors have less surface torque to rotate themselves back to the easy axis. The response time is, therefore, longer due to the relaxation time required for the boundary directors back to the final position.

When a high field is suddenly applied upon or removed from a cell, one cannot ignore the shear flow effect. As show in Figure 1.2 and 1.3, the shear flow effect influences the transient behavior of the LC directors with hard boundary condition and can be seen from the optical response. What is the outcome when the boundary directors of the cell are weakly anchored on the substrates?

A typical application of the weak anchoring boundary is the bistable nematic liquid crystal cell (BiNem) proposed by Dozov [13,14] *et al.* in 1997. It has many superior properties,

such as simple structure, fast response, high contrast ratio and wide viewing angle in addition to the permanent memory effect. The two stable states, of which the twisted angles differ by π as shown in Figures 1.4(a) and (c), can be switched through the shear flow effects and polar anchoring energy breaking on one substrate. According to the papers of Dozov, the two stable states of the BiNem cell are the U state and the T state. The upper substrate is treated to have strong polar anchoring energy with high pretilt angle, and the bottom substrate has weak polar anchoring energy and the pretilt angle is nearly zero. If the field is larger than the critical electric field, which is defined as the anchoring energy breaking of the bottom substrate, the directors near the bottom substrate are vertical, which is the D state and shown in Figure 1.4 (b). After the field is removed, the directors relax to either one of the bistable states. From the theory proposed by Dozov, the final state selection is determined by the flow effect induced by the pulse. Fast switching off the field creates a strong shear flow and the cell relaxes to the T state (Figure 1.4 (d) ~ (g)). Slowly switching off the field does not induce enough shear flow and the cell goes back to the U state (Figure 1.4 (d), (h) and (i)). This example shows the application of the shear flow effect with weak anchoring boundary.

1.3 Aims of this research

Rencently, our group has done many investigations on the dynamical behavior for different LCD modes. Dr. Li-Yi Chen [6-9] explored the influence of the flow effect on the dynamical behavior of homeotropic-like LC cells. He found that the optical-bounce phenomenon, which was originally discovered in the TN-LC cell, also appears in the rising period of the chiral-hoemotropic and pure homeotropic liquid crystal cells. The optical-bounce behavior is caused by the flow-induced twist deformation. He proposed that the response time of the homeotropic-like cell can be improved by a larger twist elastic constant. Furthermore, based on the observation of the transient transmittance of the pure homeotropic cell, he predicted the existence of two stable states in the homeotropic liquid crystal cell and demonstrated a new bistable liquid crystal device which can operate between three states. Afterward, Dr. Chih-Yung Hsieh [10-12] explored the boundary effects on the dynamical behavior of three classes of liquid crystal cells whose boundary directors are not precisely normal to the substrates: the quasi-homeotropic liquid crystal (QHLC) cell, the bistable chiral QHLC cell and $\pi/2$ bistable chiral QHLC cell. The optical oscillation (double-bounce phenomenon) in the QHLC cells during the rising period originates from not only the flow effect of liquid crystals but also the complicated alignment condition, which is

a combination of the deviation and azimuthal alignment and the asymmetrical polar alignment. The flow effect of liquid crystals and the asymmetrical polar alignment condition are important factors to achieve the switching bistabiliy of the bistable chiral QHLC cell. Hsieh also presented an electric switching $\pi/2$ bistable chiral QHLC cell with low driving voltage [12].

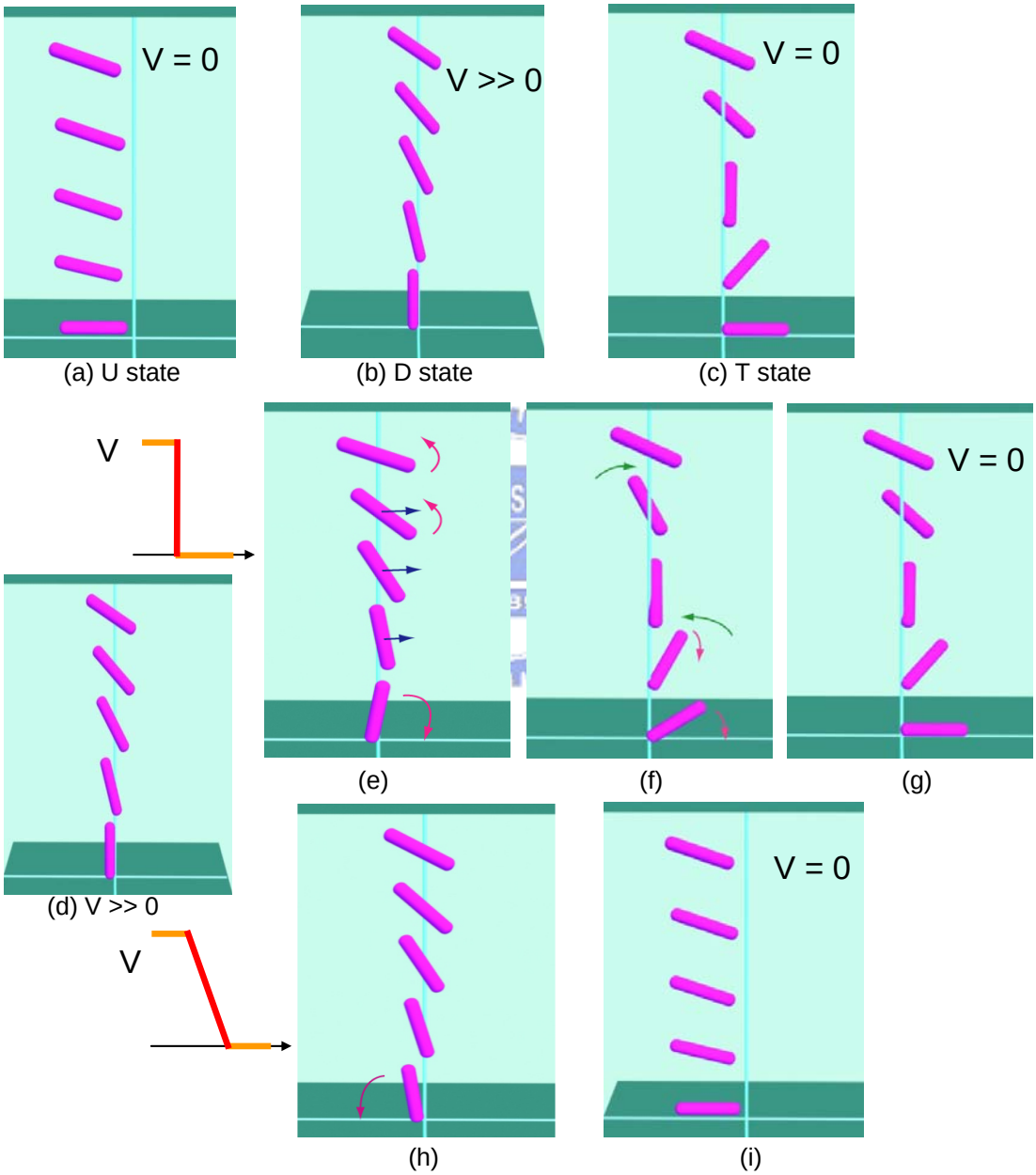

Figure 1.4 The configurations of the BiNem cell: (a) Uniform state (U state), (b) Deformed state (D state), (c) Twisted state (T state). U state and T state are the stable states at V = 0V and (b) is under an applied voltage. (d) – (g) show that the fast switching off the field creates a strong shear flow and the cell relaxes to the T state. (h) and (i) show that the slowly switching off the field does not induce enough shear flow and the cell goes back to the U state.

In this dissertation, we consider the boundary directors to be non-rigidly anchored on the substrates. The interfacial potential between the boundary directors and the alignment layer is called the surface free energy density, or the anchoring energy density. For simplicity, it can be determined by the coordinate of the easy axis (the minimum of the surface free energy density) and the anchoring energy coefficients. In Chapter 2, we first review the nemato-hydrodynamic theory and the models of the anchoring energy density. In Chapter 3, we investigate and propose methods to measure the interfacial parameters including the pretilt angle of the easy axis in the reflective vertically aligned (VA) LCD and the anchoring energy coefficients of homogeneous and homeotropic cells. After that, we combine the shear flow effect and the non-rigid boundary condition. In Chapter 4, we study the BiNem cell by adopting the weak anchoring in one of the substrates and using flow effect to achieve the switching. Several distinct dynamic behaviors appear. The mechanisms of these behaviors are explicitly explained through the tilt and azimuthal angles of the surface director on the weak anchoring boundary in the dynamic process. In Chapter 5, we propose a bistable mode—bistable chiral-tilted homeotropic nematic LC cell, BHN. The two stable states are the tilted homeotropic state and the twisted state. The main switching mechanisms are achieved by the shear flow effect together with the anisotropic properties of the dual-frequency LC material. Finally, in Chapter 6, a summary and future scopes are made.

References of Chapter 1

[1] A. Rapini and M. Papoular, J. Phys. (Paris) Colloq., **30**, C4-54, (1969).

[2] P. G. de Gennes and J. Prost, *The Physics of Liquid Crystals*. Clarendon Press, second edition, 1993.

[3] S. Chandrasekhar. *Liquid Crystals*. Cambridge University Press, second edition, 1992.

[4] C. Z. van Doorn., *J. Appl. Phys.*, **46**, 3738, (1975).

[5] D. W. Berreman,. *J. Appl. Phys.*, **46**, 3746, (1975).

[6] Shu-Hsia Chen and Li-Yi Chen, Appl. Phys. Lett., **75**, 3491, (1999).

[7] L.Y. Chen and S.H. Chen, J. SID, **7**, 289, (1999).

[8] Li-Yi Chen and Shu-Hsia Chen, Jpn. J. Appl. Phys., **39**, L368, (2000).

[9] Chih-Yung Hsieh and Shu-Hsia Chen, Jpn. J. Appl. Phys., **41**, 5264, (2002).

[10] Li-Yi Chen and Shu-Hsia Chen, Appl. Phys. Lett., **74**, 3779, (1999).

[11] Chih-Yung Hsieh and Shu-Hsia Chen, Appl. Phys. Lett., **83**, 1110, (2003).

[12] Chih-Yung Hsieh and Shu-Hsia Chen, Jpn. J. Appl. Phys., **42**, L1330, (2003).

[13] I. Dozov, M. Nobili, and G. Durand, Appl. Phys. Lett., **70**, 1179, (1997).

[14] I. Dozov and G. Durand, Liquid Crystals Today, **8**, 2, (1998).

Chapter 2

Theory

In this chapter, we will discuss the theory of the dynamic behavior of nematic liquid crystals and the anchoring properties of LC directors on the boundary. First, we will give a brief review of the theory of elasticity [1,2], which is used to characterize the static spatial director field, and nemato-hydrodynamic theory [3,4], which is applied to deal with the fluid motion of nematic liquid crystals. Then, we study the anchoring properties of the boundary and introduce several models of the anchoring energy density proposed in the literatures.

2.1 The continuum theory for nematic liquid crystal

Rigid rods are the simplest type of objects used to describe nematic LC molecules behaviors. The average direction of the alignment of certain amount molecules is along one common direction, which is called director ($\vec{n}$). It is uniaxial with $|\vec{n}| = 1$ and $\vec{n} = -\vec{n}$. The continuum theory for the nematic liquid crystal is under the assumption that $\vec{n}$ varies slowly and smoothly with respect to the position. We applied this theory to investigate the static and dynamical behavior of nematic liquid crystals under external optical, electric or magnetic fields.

2.1.1 Theory of Elasticity: Oseen-Zöcher-Frank theory

For an incompressible fluid and an isothermal deformation of the nematic liquid crystals, the total elastic free energy (F_{total}) of the system can be written as:

$$F_{total} = \int_V f_{bulk}\, dV + \int f_{surface}\, dS \qquad (2.1)$$

where f_{bulk} is the elastic free energy per unit volume and $f_{surface}$ is the surface free energy per unit area.

In this section, we only focus at the bulk liquid crystals. The elastic free energy density of the deformed nematic liquid crystals can be written as:

$$f_{bulk} = \frac{1}{2}[k_{11}(\nabla \cdot \vec{n})^2 + k_{22}(\vec{n} \cdot \nabla \times \vec{n} + q_0)^2 + k_{33}(\vec{n} \times \nabla \times \vec{n})^2] \tag{2.2}$$

where k_{11}, k_{22} and k_{33} are the splay, twist and bend elastic constants, respectively. q_0 is $2\pi/p$, where p is the pitch of the helix. For an untwisted nematic liquid crystals, q_0 is equal to 0, the pitch of the helix approaches to infinity ($p = \infty$). Equation (2.1) is derived from considering the curvature strains of the director. Other types of deformation either do not change the elastic free energy or are forbidden due to the symmetry of the liquid crystals and the absence of polarity (head to tail symmetry). It also neglect higher order terms because only the small deformations are considered. That is, only the quadratic terms are included in the elastic free energy density which resembles to the Hook's law.

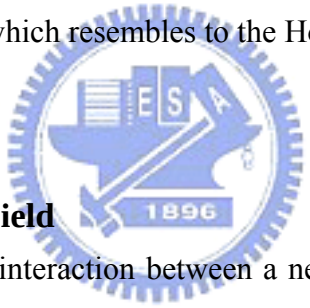

LC Directors in the Electric Field

Let's consider the dielectric interaction between a nematic LC director and the electric field. For an applied electric field (DC or low-frequency) $\vec{E}$, the displacement $\vec{D}$ may be rewritten as:

$$\vec{D} = \varepsilon_0 \varepsilon_\perp \vec{E} + \varepsilon_0 (\varepsilon_{//} - \varepsilon_\perp)(\vec{n} \cdot \vec{E})\vec{n} \,. \tag{2.3}$$

The electric energy density is

$$f_{elec} = -\frac{1}{2}\vec{D} \cdot \vec{E} = -\frac{1}{2}\varepsilon_0 \varepsilon_\perp E^2 - \frac{1}{2}\varepsilon_0 \Delta\varepsilon (\vec{n} \cdot \vec{E})^2 \,. \tag{2.4}$$

Note that the first term on the right-hand side of Eq. (2.4) is independent of the orientation of the director axis. Therefore, the electric torque acting on the LC directors is

$$\begin{aligned} \tau_E = \vec{n} \times \vec{f}_E &= \vec{n} \times \left(-\frac{\partial f_{elec}}{\partial \vec{n}} \right) = \varepsilon_0 \Delta\varepsilon (\vec{n} \cdot \vec{E})(\vec{n} \times \vec{E}) \\ &= \frac{1}{2}\varepsilon_0 \Delta\varepsilon E^2 \sin(2\xi). \end{aligned} \tag{2.5}$$

where ξ is the angle between the director and the electric field shown in Figure 2.1. When the director is free to rotate, the torque is maximum when the angle between the director and the direction of the electric field is 45°.

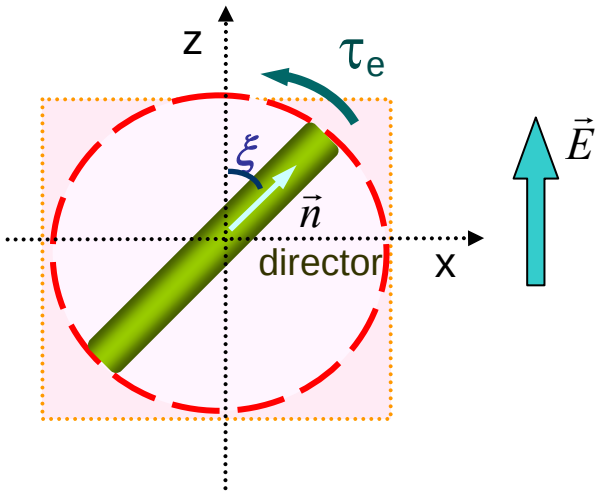

Figure 2.1 Sketch of the geometry and the coordinates for a free director under an applied electric field. The induced torque is related to the angle between the director and the direction of the electric field.

Euler-Lagrange equation for a LC system under the external applied field

Let's consider a nematic liquid crystal slab of thickness d in an external electric field $\vec{E}$. For simplicity, we have supposed that all variable depend only on the z-coordinate, the total free energy per unit area of the system is given by

$$f_{total}[\varphi(z)] = \int_{-d/2}^{d/2} f_{bulk}[\varphi(z), \varphi'(z); z]dz + f_{s1}(\varphi_1) + f_{s2}(\varphi_2). \quad (2.6)$$

where φ characterizes the deformation, and $\varphi' = d\varphi/dz$. f_{bulk} is the bulk elastic free energy density and $f_{s1}(\varphi_1)$ and $f_{s2}(\varphi_2)$ the surface energy density, with $\varphi_1 = \varphi(-d/2)$, $\varphi_2 = \varphi(d/2)$.

If $\tilde{\varphi}(z)$ is the function minimizing the function $f_{total}[\varphi(z)]$. $\varphi(z)$ is chosen to close to $\tilde{\varphi}(z)$, in the following way

$$\varphi(z) = \tilde{\varphi}(z) + \alpha\upsilon(z),$$

where $\upsilon(z) \in C_1$ is an arbitrary function and α a small parameter.

$$\left[\frac{df_{total}}{d\alpha}\right]_{\alpha=0}=\left\{\frac{d}{d\alpha}\int_{-d/2}^{d/2}f_{bulk}[\varphi(z),\varphi'(z);z]+\frac{df_{s1}(\varphi_1)}{d\alpha}+\frac{df_{s2}(\varphi_2)}{d\alpha}\right\}_{\alpha=0},$$

$$\frac{df_{bulk}}{d\alpha}=\frac{\partial f_{bulk}}{\partial\varphi}\frac{\partial\varphi}{\partial\alpha}+\frac{\partial f_{bulk}}{\partial\varphi'}\frac{\partial\varphi'}{\partial\alpha}$$

where

$$\frac{\partial f_{bulk}}{\partial\varphi'}\upsilon'=\frac{d}{dz}\left[\frac{\partial f_{bulk}}{\partial\varphi'}\upsilon\right]-\left[\frac{d}{dz}\frac{\partial f_{bulk}}{\partial\varphi'}\right]\upsilon$$

$$\begin{aligned}\left[\frac{df_{total}}{d\alpha}\right]_{\alpha=0}=&\left\{\int_{-d/2}^{d/2}\left[\frac{\partial f_{bulk}}{\partial\varphi}-\frac{d}{dz}\frac{\partial f_{bulk}}{\partial\varphi'}\right]\upsilon(z)dz\right\}_{\alpha=0}+\left\{\left[\left(\frac{\partial f_{bulk}}{\partial\varphi'}\right)_{d/2}+\frac{df_{s2}}{d\varphi_2}\right]\upsilon(d/2)\right\}_{\alpha=0}\\&+\left\{\left[\left(\frac{\partial f_{bulk}}{\partial\varphi'}\right)_{-d/2}+\frac{df_{s1}}{d\varphi_1}\right]\upsilon(-d/2)\right\}_{\alpha=0}\end{aligned}\tag{2.7}$$

Since $\tilde{\varphi}(z)$ minimizes f_{total}, we deduce that

$$\delta f_{total}=\left[\frac{df_{total}}{d\alpha}\right]_{\alpha=0}=0,\quad\forall\,\upsilon(z)\in C_1,$$

Consequently, from Eq. (2.7), It follows that $\tilde{\varphi}(z)$ is the solution of the Euler-Lagrange equation:

$$\frac{\partial f_{bulk}}{\partial\tilde{\varphi}}-\frac{d}{dz}\frac{\partial f_{bulk}}{\partial\tilde{\varphi}'}=0,\qquad\forall z\in(-d/2,d/2).\tag{2.8}$$

And satisfies the boundary conditions

$$-\frac{\partial f_{bulk}}{\partial\tilde{\varphi}'}+\frac{df_{s1}}{d\varphi_1}=0,\quad-\frac{\partial f_{bulk}}{\partial\tilde{\varphi}'}+\frac{df_{s2}}{d\varphi_2}=0,\tag{2.9}$$

for $z=-d/2$ and $z=d/2$.

2.1.2 Hydrodynamic theory: Ericksen-Leslie theory

In the following, we will give a brief description of Ericksen-Leslie theory. First, we consider the medium to be incompressible and at constant temperature. The director is assumed to be of constant magnitude. Let the material volume be *V* bounded by a surface *A*. The conservation laws take the following form:

Conservation of mass

$$\frac{d}{dt}\int_V \rho dV = 0 , \tag{2.10}$$

where ρ is the density of liquid crystals.

Conservation of linear momentum

$$\frac{d}{dt}\int_V \rho v_i dV = \int_V f_i dV + \int_A t_{ji} dA_j , \tag{2.11}$$

where v_i is the linear velocity of the director, f_i is the body force per unit volume and t_{ji} the stress tensor.

Conservation of energy

$$\frac{d}{dt}\int_V (\frac{1}{2}\rho v_i v_i + U + \frac{1}{2}\rho_1 \dot{n}_i \dot{n}_i) dV = \int_V (f_i v_i + G_i \dot{n}_i) dV + \int_A (t_i v_i + s_i \dot{n}_i) dA_j , \tag{2.12}$$

where ρ_1 is a material constant having the dimension of moment of inertia per unit volume (ML^{-1}), U the internal energy per unit volume, G_i the external director body force (which has the dimensions of torque per unit volume since n_i has been chosen to be dimensionless), $t_i=t_{ji}v_j$ the surface force per unit area acting across the plane whose unit normal is v_j, and $s_i=\pi_{ji}v_j$ the director surface force (which has the dimensions of torque per unit area). We assume here that there are no heat sources or sinks.

Oseen's equation

$$\int_V \rho \ddot{n}_i dV = \int_V (G_i + g_i) dV + \int_A \pi_{ji} dA_j , \tag{2.13}$$

where g_i is the intrinsic director body force, which has the dimensions of torque per unit volume and whose existence is independent of G_i.

Converting surface integrals into volume integrals and simplifying, (2.10)-(2.13) lead to the following four differential equations:

Conservation of mass: $\dot{\rho} = 0$ (2.14)

Conservation of linear momentum: $\rho \dot{v}_i = f_i + t_{ji,j}$ (2.15)

Conservation of energy: $\dot{U} = t_{ji} d_{ij} + \pi_{ji} N_{ij} - g_i N_i$ (2.16)

Oseen's equation: $\rho \ddot{n}_i = G_i + g_i + \pi_{ji,j}$ (2.17)

where

$$t_{ji} - \pi_{kj} n_{i,k} + g_j n_i = t_{ij} - \pi_{ki} n_{j,k} + g_i n_j ,$$

$$N_i = \dot{n}_i - w_{ik} n_k ,$$

$$N_{ij} = \dot{n}_{i,j} - w_{ik} n_{k,j} ,$$

$$2d_{ij} = v_{i,j} + v_{j,i} ,$$

$$2w_{ij} = v_{i,j} - v_{j,i} ,$$

N_i may be interpreted as the angular velocity of the director relative to that of the fluid. It should be emphasized that the stress tensor t_{ji} is asymmetric. When n_i= 0, (2.14)-(2.17) reduce to the familiar equations of hydrodynamics for an isotropic fluid.

The constitutive equation for the qualities g_i, t_{ji} and π_{ji} was developed by Leslie who assumed that these qualities were single-valued function of n_i, ni,j , N_i and d_{ij} and separated t_{ji} and g_i into a static (or elastic) part and a hydrodynamic (or viscous) part.

$$t_{ji} = t^0_{ji} + t'_{ji} , \quad g_i = g^0_i + g'_i$$

where the superscript 0 denotes the isothermal static deformation value and the prime denotes the hydrodynamic part, g'_i is the hydrodynamic part of the director body force, t'_{ji} is the hydrodynamic part of the stress tensor,

$$t^0_{ji} = -p\delta_{ij} - \frac{\partial f_{bulk}}{\partial n_{k,i}} n_{k,i}$$

$$g^0_i = \gamma n_i - \beta_j n_{i,j} - \frac{\partial f_{bulk}}{\partial n_i}$$

$$\pi_{ji} = \pi^0_{ji} + \pi'_{ji} = \pi_{ji} = \beta_j n_i + \frac{\partial f_{bulk}}{\partial n_{i,j}}$$

$$t'_{ji} = \alpha_1 n_k n_m d_{km} n_i n_j + \alpha_2 n_j N_i + \alpha_3 n_i N_j + \alpha_4 d_{ji} + \alpha_5 n_j n_k d_{ki} + \alpha_6 n_i n_k d_{kj} \qquad (2.18)$$

$$g'_i = -\gamma_1 N_i - \gamma_2 n_j d_{ji}$$

$$\gamma_1 = \alpha_3 - \alpha_2 \quad (\gamma_1 : \text{ rotational viscosity}) \qquad (2.19)$$

$$\gamma_2 = \alpha_6 - \alpha_5$$

where p, γ, and β_j are arbitrary constants, π'_{ji} is the hydrodynamic part which is equal to zero, $\alpha_1 \sim \alpha_6$ represent the six Leslie coefficients of viscosity of a nematic liquid crystals.

The *Paraodi's relation*: $\alpha_2 + \alpha_3 = \alpha_6 - \alpha_5$ (2.20)

In general, the shear viscous coefficients (Miesowicz's coefficients, η_1, η_2, η_3, η_{13}) and the rotational coefficients can be measured by experiment, the Leslie coefficients then can be derived by shear viscous coefficients. The relationship between the Miesowicz coefficients and the Leslie coefficients of viscosity can be established by substituting the director components and velocity gradients into Eq. (2.18) together with the rotational viscosity (2.19) and the Parodi's relation (2.20).

$$\eta_1 = \frac{1}{2}(-\alpha_2 + \alpha_4 + \alpha_5),$$

$$\eta_2 = \frac{1}{2}(\alpha_3 + \alpha_4 + \alpha_6),$$

$$\eta_3 = \frac{1}{2}\alpha_4,$$

$$\eta_{12} = \alpha_1.$$

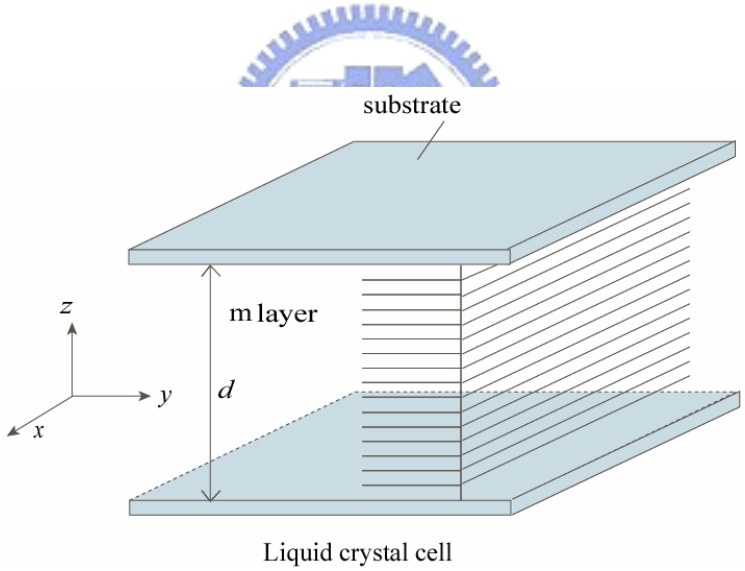

Figure 2.2 The liquid crystal cell, which has infinite extension in the x and y directions, is bounded at $z = 0$ and $z = d$. The layer is divided into m equally spaced sub-layers. Fluid velocities and director orientation are functions of z and t only.

The equations for the one-dimension flow problem

In our simulation, we suppose that the liquid crystal layer extends to infinity in x-y plane and is bounded at $z = 0$ and $z = d$ (see Figure 2.2) and the applied electric field is applied along the z-coordinate. Furthermore, we assume all quantities, such as fluid velocities, director orientation, voltage potential and electric field, depend only on the z-coordinate.

We only consider the planar flow of liquid crystals and the z-component of the velocity is assumed to be zero and the boundary directors are rigidly anchored on the substrates and the velocity there is also assumed to be zero.

Suppose the LC is an impressible material, in the isothermal process:

$$\vec{n} = \vec{n}(z,t), \quad \vec{v} = \vec{v}(z,t)$$

$$n_{i,x} = n_{i,y} = v_{i,x} = v_{i,y} = 0\,, (i = x, y, z),$$

Therefore,

$$d_{xz} = d_{zx} = \frac{1}{2} v_{x,z}\,, \quad d_{yz} = d_{zy} = \frac{1}{2} v_{y,z}\,,$$

$$w_{xz} = -w_{zx} = \frac{1}{2} v_{x,z}\,, \quad w_{yz} = -w_{zy} = \frac{1}{2} v_{y,z}$$

$$d_{x,y} = d_{y,x} = d_{x,x} = d_{y,y} = d_{z,z} = 0\,, \quad w_{x,y} = w_{y,x} = w_{x,x} = w_{y,y} = w_{z,z} = 0$$

$$n_k n_m d_{km} = n_y n_z v_{y,z} = n_x n_z v_{x,z}\,, \quad n_z n_k d_{kx} = n_z^2 d_{z,x} = \frac{1}{2} n_z^2 v_{x,z}\,, \quad n_x n_k d_{kz} = \frac{1}{2}(n_x n_y v_{y,z} + n_x^2 v_{x,z})\,,$$

$$N_x = \dot{n}_x - \frac{1}{2} v_{x,z} n_z\,, \quad N_y = \dot{n}_y - \frac{1}{2} v_{y,z} n_z\,, \quad N_z = \dot{n}_z + \frac{1}{2} v_{x,z} n_x + \frac{1}{2} v_{y,z} n_y\,,$$

The one-dimensional conservation of linear momentum can be written as:

$$\begin{aligned} \rho\, \dot{v}_x = \frac{\partial}{\partial z}[&(\alpha_2 n_z \dot{n}_x + \alpha_3 n_x \dot{n}_z) + (\alpha_1 n_y n_z^2 n_x + \frac{1}{2}\alpha_3 n_y n_x + \frac{1}{2}\alpha_6 n_x n_y)\frac{\partial v_y}{\partial z} \\ &+ (\alpha_1 n_x^2 n_z^2 - \frac{1}{2}\alpha_2 n_z^2 + \frac{1}{2}\alpha_3 n_x^2 + \frac{1}{2}\alpha_4 + \frac{1}{2}\alpha_5 n_z^2 + \frac{1}{2}\alpha_6 n_x^2)\frac{\partial v_x}{\partial z}] \end{aligned} \tag{2.21}$$

$$\begin{aligned} \rho\, \dot{v}_y = \frac{\partial}{\partial z}[&(\alpha_2 n_z \dot{n}_y + \alpha_3 n_y \dot{n}_z) + (\alpha_1 n_y n_z^2 n_x + \frac{1}{2}\alpha_3 n_x n_y + \frac{1}{2}\alpha_6 n_x n_y)\frac{\partial v_x}{\partial z} \\ &+ (\alpha_1 n_y^2 n_z^2 - \frac{1}{2}\alpha_2 n_z^2 + \frac{1}{2}\alpha_3 n_y^2 + \frac{1}{2}\alpha_4 + \frac{1}{2}\alpha_5 n_z^2 + \frac{1}{2}\alpha_6 n_y^2)\frac{\partial v_x}{\partial z}] \end{aligned} \tag{2.22}$$

The equation of motion of the directors:

$$\rho_1 \ddot{n}_x = \lambda n_x - \frac{\partial f_{bulk}}{\partial n_x} + \frac{\partial}{\partial z}\frac{\partial f_{bulk}}{\partial n_{x,z}} - \gamma_1 \dot{n}_x - \alpha_2 n_z \frac{\partial v_x}{\partial z} \tag{2.23}$$

$$\rho_1 \ddot{n}_y = \lambda n_y - \frac{\partial f_{bulk}}{\partial n_y} + \frac{\partial}{\partial z}\frac{\partial f_{bulk}}{\partial n_{y,z}} - \gamma_1 \dot{n}_y - \alpha_2 n_z \frac{\partial v_y}{\partial z} \tag{2.24}$$

$$\rho_1 \ddot{n}_z = \lambda n_z - \frac{\partial f_{bulk}}{\partial n_z} + \frac{\partial}{\partial z}\frac{\partial f_{bulk}}{\partial n_{z,z}} - \gamma_1 \dot{n}_z - \alpha_3 n_x \frac{\partial v_x}{\partial z} - \alpha_3 n_y \frac{\partial v_y}{\partial z} + \varepsilon_0 \Delta\varepsilon E_z^2 n_z \tag{2.25}$$

where λ is the Lagrange multiplier which is determined by the constrain, $|\vec{n}| = 1$.

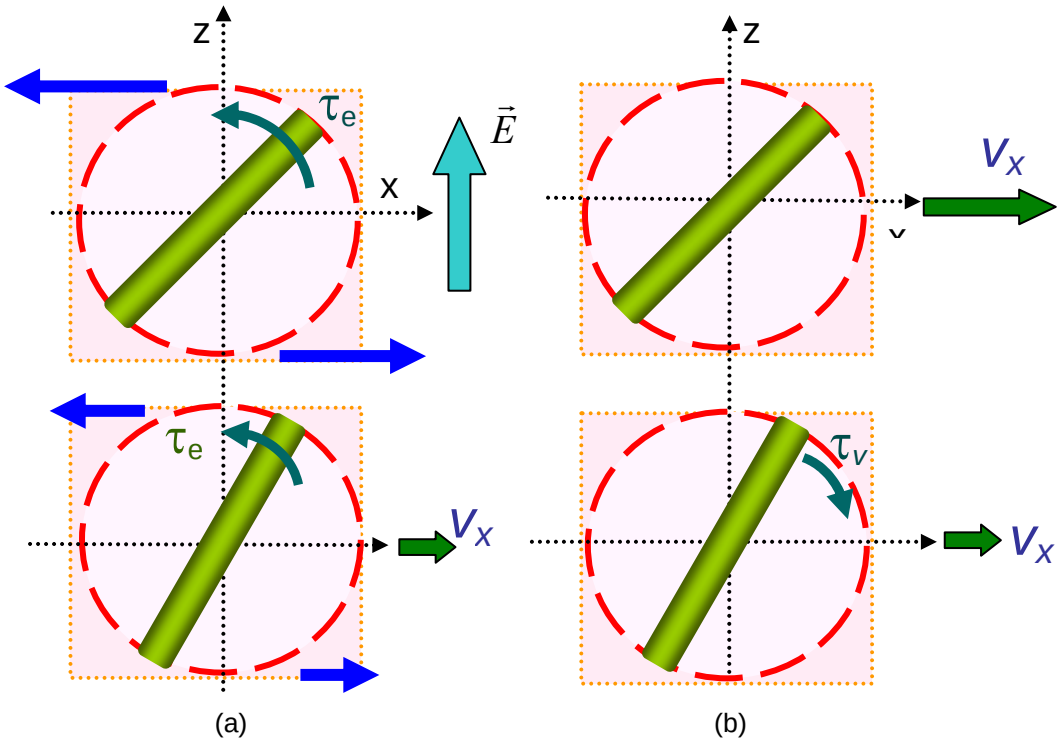

Figure 2.3 The liquid crystal director under an external electric field. The director rotates by the electric field and induces the movement of the center of mass of the director. The movement of the director will influence the rotation of the director.

In most cases, the liquid crystal system may be regarded as a strongly damping oscillator and the influence of the inertia terms is very small comparison with the viscous terms. We may assume that, after a change of the field strength, a new velocity pattern is established almost instantaneously. Therefore, the inertia terms can be neglected without losing significant effects and the left side of Eq. (2.21) to (2.25) equals zero.

Figure 2.3 illustrates the flow effects between two layers. Due to the different tilt angles of the directors, the electric torques acting on the directors, which can be derived from Eq. (2.5), are not equal. Therefore, there are two unequal shear forces acting on the interface between two layers. Since the liquid crystal is assumed to satisfy the continuum theory and obeys the conservation laws and Oseen's equation, Eq. (2.21) to (2.25), there is a relative velocity between these two layers, which is illustrated in Figure 2.3 (a). On the other hand, if there is a relative velocity between two layers, an induced torque is produced which is shown in Figure 2.3 (b). These dynamic behaviors are coupled together.

If we assume there is no flow phenomenon and ignore the inertia term in the motion equation of director, we obtain the general form of the static deformation equation from Eq. (2.23) to (2.25):

$$\frac{\partial}{\partial z}\frac{\partial f_{bulk}}{\partial n_{i,z}} - \frac{\partial f_{bulk}}{\partial n_i} + \lambda n_i = \gamma_1 \dot{n}_i - G_i . \tag{2.26}$$

The one dimensional response time (rising time and relaxation time) can be estimated by this equation when the applied forces are not large enough to induce the flow effects.

2.2 Models of the anchoring energy density

The anchoring of liquid crystal (LC) directors at substrates plays a very important role in the performance characteristics of any liquid crystal display (LCD), such as viewing angle, contrast ratio and response time. In the modeling of LCD, the anchoring energy must be included in the calculation. To describe the surface effect, Rapini and Papoular [5] (RP) have introduced a simple phenomenological expression for the interfacial surface anchoring energy per unit area, f_s, which describes the interaction between the nematic director and substrate of homeotropic anchoring: $f_s = \frac{1}{2} W \sin^2(\theta)$, where θ is the polar angle of the director and W is the anchoring energy coefficient, which determines the ability of the director to deviate from the easy axis. Subsequently, many attempts had been carried out to generalize the RP model in order to describe the planar and tilt anchoring[6-9]. Becker *et al.*[6] considered a surface with weak polar and strong azimuthal anchoring. Hirning *et al.*[7] combined the polar and azimuthal anchoring to an interfacial energy without correlations between them. Sugimura *et al.*[8-10] used a single coupling constant to describe the interfacial energy. They suggested that the interfacial energy should not be separated into the polar and azimuthal surface anchoring energies, which are independent of each other, as is conveniently carried out. Zhao *et. al.*[11,12] generalized an RP-type anchoring energy formula with two anchoring coefficients and an orthonormal vector triplet through a second-order spherical harmonic expansion. These models are discussed in the following sections.

2.2.1 Rapani-Popular model

The interfacial potential of between the surface director and the homeotropic alignment for the Rapani-Papoular model is:

$$f_s = \frac{1}{2} W \sin^2(\theta), \tag{2.25}$$

where θ is the polar angle of the director and W is the anchoring energy coefficient.

Figure 2.4 shows the interfacial potential as a function of the surface director. The surface director is represented by the corresponding points on the x-y plate, which is the projection of the surface directors from z direction. The height in the diagram is the surface anchoring energy density f_s. The interfacial potential is symmetric in the azimuthal direction and the tilt angle of the easy axis is 90°.

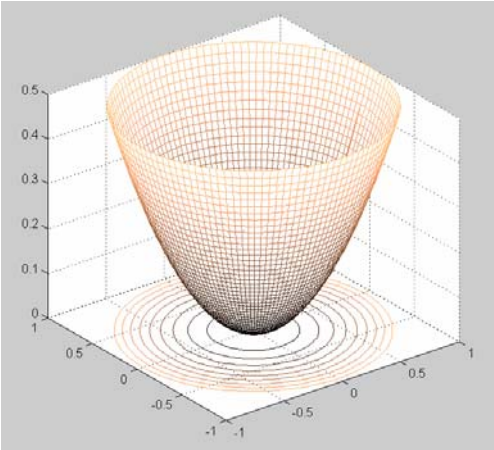

Figure 2.4 The interfacial potential of Rapani-Papoular model

2.2.2 Other models

On the other hand, one of the popular formulas used in the literatures is shown as [7]:

$$f_s = \frac{1}{2} W_\theta \sin^2(\alpha - \alpha_e) + \frac{1}{2} W_\phi \sin^2(\phi - \phi_e), \tag{2.26}$$

where α_e and ϕ_e are the tilt angle and the azimuthal angle of the easy axis. The f_s with α_e=0°, ϕ_e=0° and W_θ =1, W_ϕ =0.5 is plotted in the Figure 2.5. The first and the second column are the polar and azimuthal anchoring energy density of f_s, respectively. The third column is the combination of these two energies. The height in the first row and the colors in the second row represent the values of anchoring energy density. We find it oscillates extremely in the azimuthal direction when α near 90° as shown in (b) and (e). This seems

unreasonable and results in a non-smooth shape in the surface anchoring energy density in (c) and (f). Moreover, if the pretilt angle is not zero, the surface free energy should have a minimum at the location of the easy axis. However, from Eq. (2.26), the surface free energy density has two minimum at $\alpha = \alpha_e$ and $\alpha = 180° - \alpha_e$. This is irrational since the directors which have the property of $\vec{n} = -\vec{n}$, should have the minimum free energy at $\alpha = \alpha_e$ and $\alpha = 180° + \alpha_e$. This contradiction can be observed in Figure 2.6 with the pretilt angle of 45°.

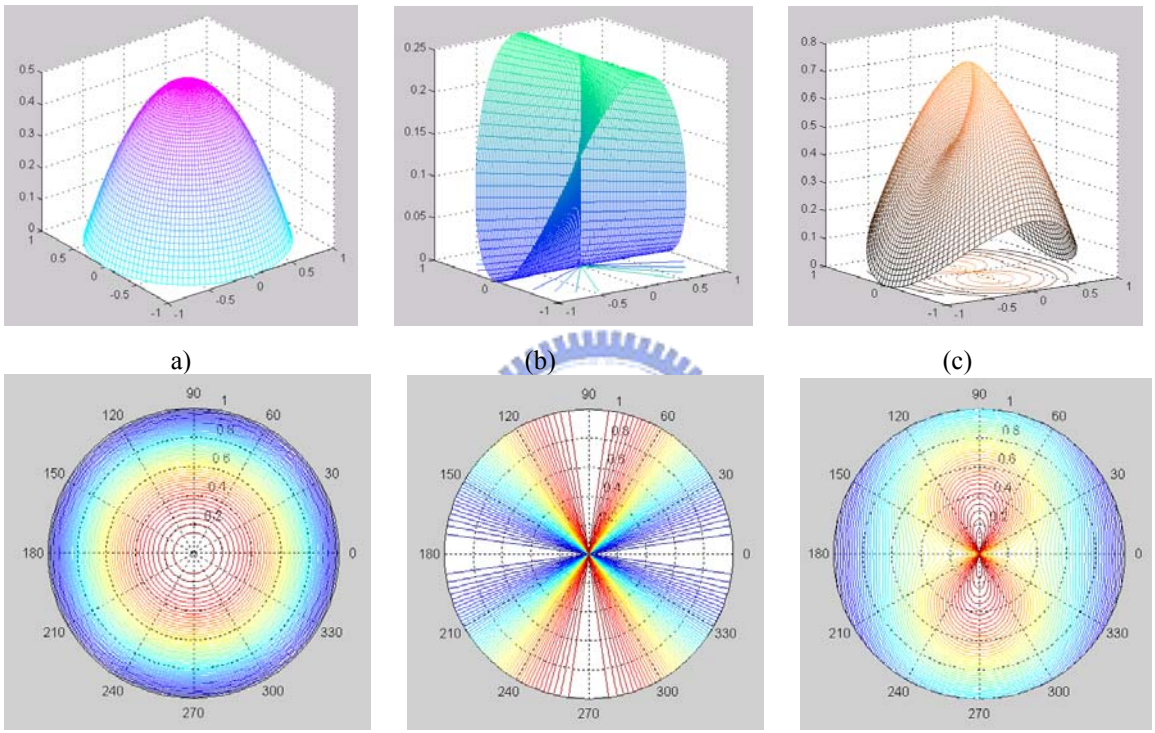

a) (b) (c)

(d) (e) (f)

Figure 2.5 The interfacial potential of $f_s = \frac{1}{2}W_\theta \sin^2(\alpha - \alpha_e) + \frac{1}{2}W_\phi \sin^2(\phi - \phi_e)$ with α_e=0°, ϕ_e=0°, W_θ=1, W_ϕ=0.5. (a), (d) and (b), (e) are the polar and azimuthal anchoring energy portions of f_s, respectively. The third column is the combination of these two energies. The height in the first row and the colors in the second row represent the values of anchoring energy.

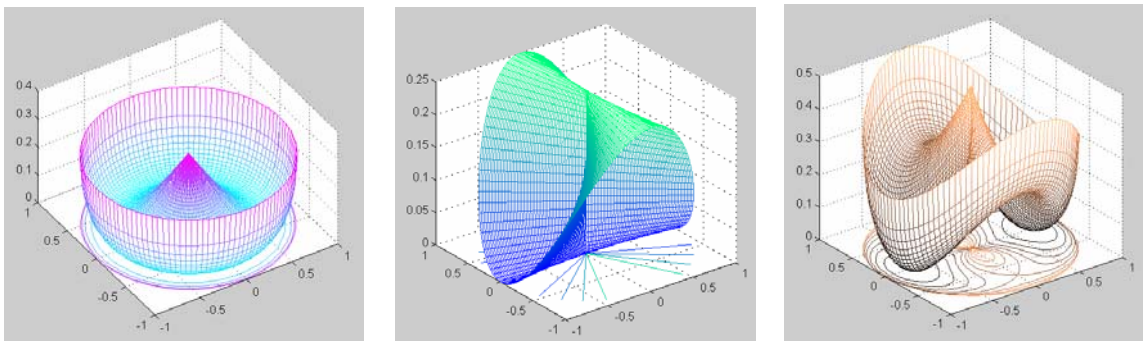

(a) (b) (c)

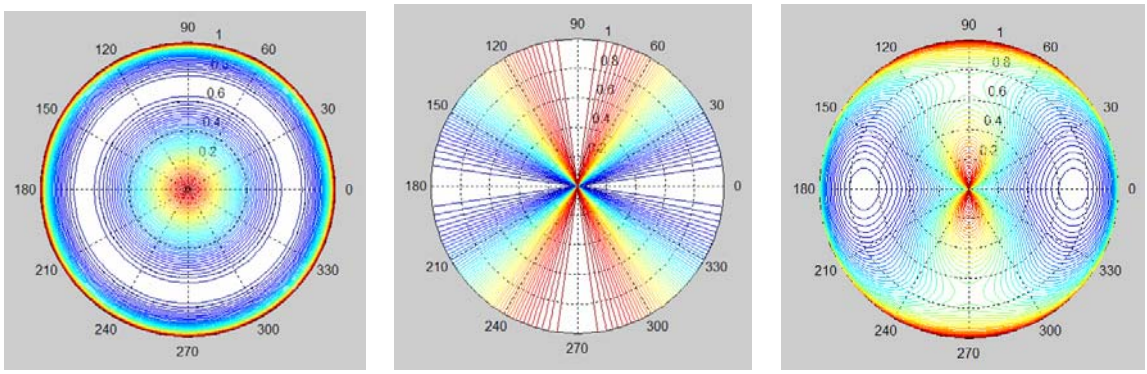

(d) (e) (f)

Figure 2.6 The interfacial potential of $f_s = \frac{1}{2}W_\theta \sin^2(\alpha-\alpha_e) + \frac{1}{2}W_\phi \sin^2(\phi-\phi_e)$ with α_e=45°, ϕ_e=0°, W_θ=1, W_ϕ=0.5

The model used by DIMOS

The surface anchoring energy density used by commercial simulator DIMOS (autronics-MELCHERS) is:

$$f_s = \frac{1}{2}W_\theta \sin^2(\alpha-\alpha_e) + \frac{1}{2}W_\phi \sin^2(\phi-\phi_e)\cos^2\alpha. \qquad (2.27)$$

With the α_e=0°, ϕ_e=0° and W_θ=1, W_ϕ=0.5, we have Figure 2.7. The shapes in (b), (e) and (c), (f) seem more reasonable compared with that of Figure 2.5 in the large α regime. However, the problem of easy axes still exists as shown Figure 2.8 (c) and (f).

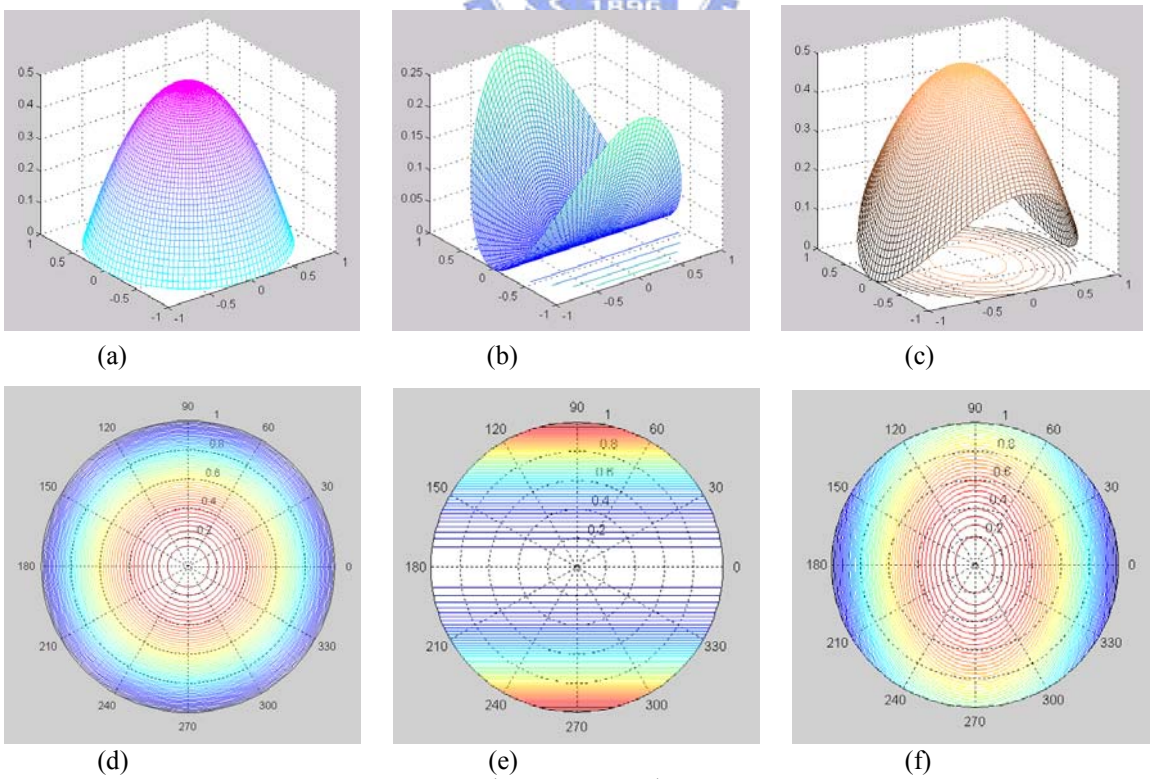

(a) (b) (c)

(d) (e) (f)

Figure 2.7 The interfacial potential of $f_s = \frac{1}{2}W_\theta \sin^2(\alpha-\alpha_e) + \frac{1}{2}W_\phi \sin^2(\phi-\phi_e)\cos^2\alpha$ with α_e=0°, ϕ_e=0°, W_θ=1, W_ϕ = 0.5

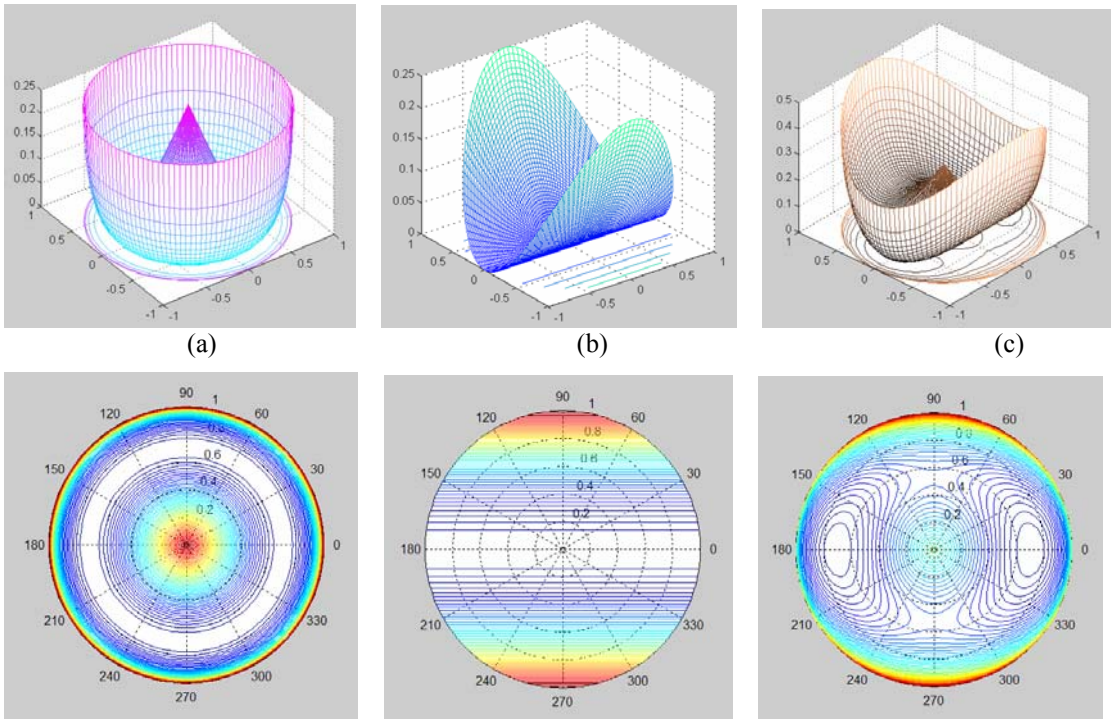

Figure 2.8 The interfacial potential of $f_s = \frac{1}{2}W_\theta \sin^2(\alpha - \alpha_e) + \frac{1}{2}W_\phi \sin^2(\phi - \phi_e)\cos^2\alpha$ with α_e=45°, ϕ_e=0°, W_θ=1, W_ϕ = 0.5

The Unified model [8-10]

The unreasonable location of the minimum free energy is solved if one used the unified model with the surface anchoring energy density shown as:

$$f_s = -\frac{1}{2}W\cos^2\zeta = -\frac{1}{2}W(\hat{n}\cdot\hat{e})^2. \tag{2.28}$$

where ζ is the angle between the easy axis $\hat{e}$ and the directors $\hat{n}$. Figure 2.9 shows the surface anchoring energy density as the pretilt decrease from 90° to 0°. However, it only uses one anchoring energy coefficient to describe the potential in the azimuthal and polar direction.

The generalized RP model [11,12]

Finally, W. Zhao *et al*. propose a model as a generalized RP model which shown as:

$$f_s = \frac{1}{2}W_{\hat{\xi}}(\hat{n}\cdot\hat{\xi})^2 + \frac{1}{2}W_\eta(\hat{n}\cdot\hat{\eta})^2. \tag{2.29}$$

where $(\hat{e},\hat{\xi},\hat{\eta})$ is an orthonormal vector triplet with Euler angles (ϕ_e,θ_e,ψ_e) with respect to $(\hat{x},\hat{y},\hat{z})$ and is shown in Figure 2.10.

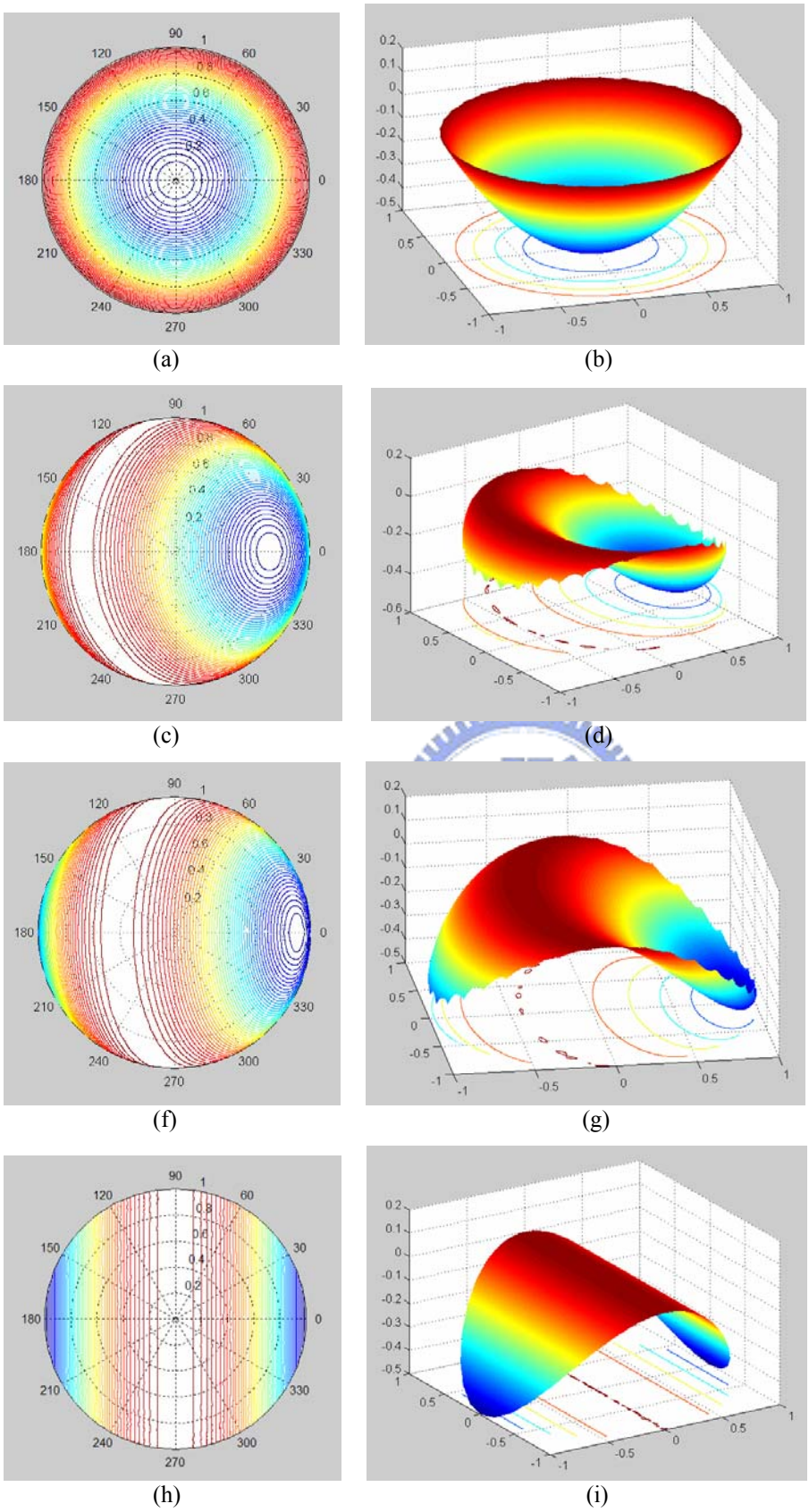

Figure 2.9 The surface anchoring energy of the unified model as the pretilt decrease from 90° (a) to 45°(c), 25°(f), and 0°(h).

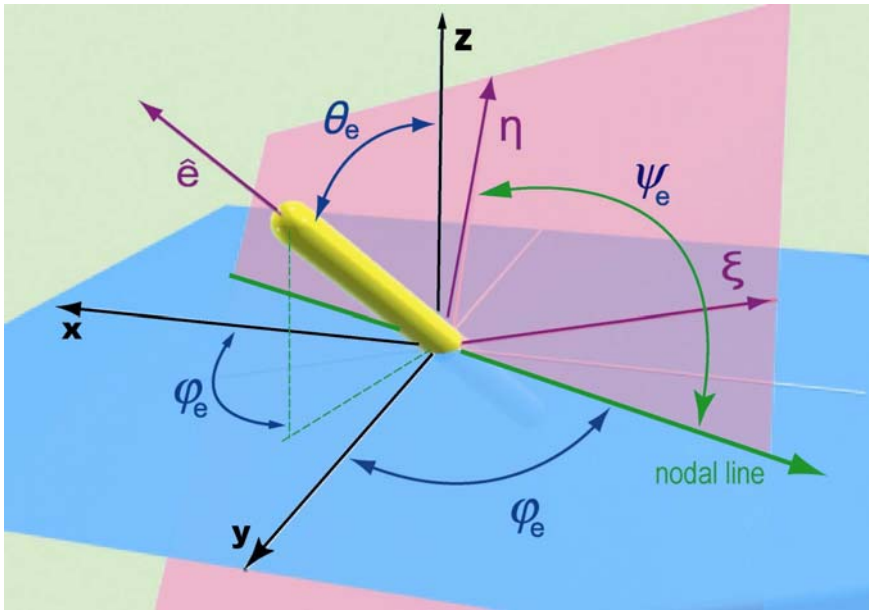

Figure 2.10 φ_e is the angle between the nodal line and y-axis, θ_e is the angle between the easy axis and the z-axis, ψ_e is the angle between the nodal line and η-axis.

W_ξ (W_η) is the energy difference between $\hat{\xi}(\hat{\eta})$ and $\hat{e}$ directions. Figure 2.11 shows the surface anchoring energy as the pretilt decrease from 90° to 0°. This model successfully solve the problem of $\vec{n} = -\vec{n}$ and have two anchoring energy coefficients to describe the movement of the surface directors.

For all these models, when the pretilt angle is close to 0° or 90° and the deviation of the surface director is small, the anchoring energy densities are alike. If we only consider the movement of the surface director in the polar direction, one simply adds the pretilt angle α_e to the RP model and the anchoring energy density becomes:

$$f_s = \frac{1}{2} W_\theta \sin^2(\alpha - \alpha_e). \tag{2.30}$$

This formula implies that the surface director is rigidly anchored in the azimuthal direction and sometimes it is also called PR model.

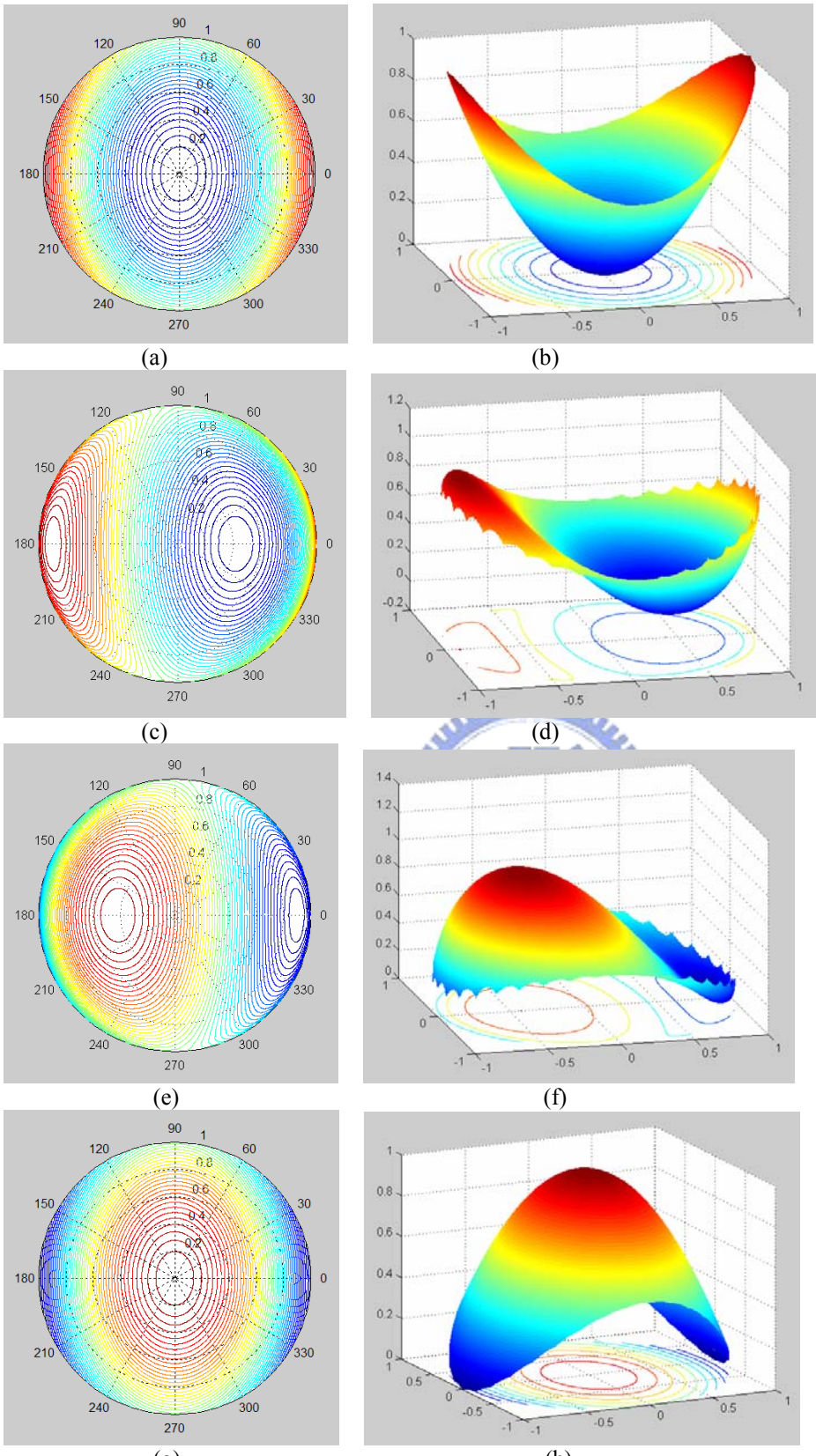

Figure 2.11 The surface anchoring energy of the unified model as the pretilt decrease from (a) to 60°(c), 25°(f), and 0°(h).

References of Chapter 2

[1] C. W. Oseen. .The theory of liquid crystals. *Trans. Faraday Soc.*, **29**, 883 (1933).

[2] F. C. Frank, .Liquid crystals: On the theory of liquid crystals.. *Discuss Faraday Soc.*, **25**, 19 (1958).

[3] J. L. Ericksen, Anisotropic fluids. *Arch. Ration. Mech. Anal.*, **4**, 231 (1960).

[4] F. M. Leslie, Some constitutive equations for liquid crystals, *Arch. Ration. Mech. Anal.*, **28**, 265 (1968).

[5] A. Rapini, and M. Papoular, J. Phys. (Paris) Colloq., **30**, C4-54, (1969).

[6] M. E. Becker, J. Nehring, and T. J. Scheffer, J. Appl. Phys., **57**, 4539, (1985).

[7] R. Hirning, W. Funk, H. R. Trebin, M. Schmidt, and H. Schmiedel, J. Appl. Phys., **70**, 4211, (1991).

[8] A. Sugimura, O. Y. Zhong-can, Phys. Rev. E., **51**, 784, (1995).

[9] A. Sugimura, G. R. Luckhurst, O. Y. Zhong-can, Phys. Rev. E., **52**, 681, (1995).

[10] A.Sugimura, T. Miyamoto, M.Tsuji and M. Kuze, Appl. Phys. Lett. **72**, 329 (1998).

[11] W. Zhao, C. X. Wu, and M. Iwamoto, Phys. Rev. E., **62**, R1481, (2000).

[12] Wei Zhao, Chen-Xu Wu and Mitsumasa Iwamoto, Phys. Rev. E, **65**, 031709, (2002).

Chapter 3

Study on the anchoring energy density

In order to understand the influence of the anchoring properties on the dynamic behaviors, we have to know the coordinates of the easy axis first. The coordinate of the easy axis means the azimuthal and the tilt angle of the easy axis. The tilt angle of the easy axis is so called the pretilt angle. Since the electric fields are usually applied in the surface normal direction, the study is focused on the behaviors of the LC directors in the polar direction. To measure the pretilt angle, several techniques of LC cells have been proposed in the literature [1–5], such as the magnetic null method [1], the crystal rotation technique[2,3], the polarizer rotation method[4] and the phase retardation measurement method [5]. These methods are accurate and reliable for the pretilt angle measurement of the transmissive cells. However, one has to modify these methods in order to measure the reflective cells, which either complicates the set-up [1–4] or limits itself to the large pre-polar angle measurement [5]. In the former part of this chapter, we propose a method to determine the pretilt angle of the VA reflective LC cells; moreover, this method can also be applied to the transmissive cells.

Once the easy axis is confirmed, we are ready to measure the anchoring properties of the LC cells. The anchoring energy density model usually used for measuring the polar anchoring energy coefficient is PR model with the formula of Eq. (2.30). The commonly used method to determine the polar anchoring energy density coefficient is the high-electric-field (HEF) method [6,7], in which the coefficient of the polar anchoring energy ($W_{\theta,RP}$) is determined within the high applied electric field regime. However, the negative $W_{\theta,RP}$ values are sometimes obtained [8]. In fact, the director distortions calculated from the RP formula do not agree well with the observations in strong external fields. Since a large applied field causes large deviation angles, the adaptability of the RP model is

questioned and the anchoring energy density requires modification. In later part of this chapter, we adopt a modified polar anchoring energy density to determine the coefficients of some non-twisted cells.

3.1 Determination of the pretilt angle of the reflective liquid crystal cells

Reflective liquid crystal display (R-LCD) has been widely used because of their low power consumption, lightweight, and outdoor readability. The characteristics of R-LCD, such as brightness, contrast ratio, and response time, are determined by the cell gap, twist angle, pretilt angle etc., and the measurements of these parameters are still developing [9-12]. Among the modes used in LCD, vertically aligned (VA) mode exhibits excellent dark state, which is a nice candidate to be used in the R-LCD e.g. LCoS (Liquid Crystal on Silicon). The pre-polar angle (measured from the substrate normal) of VA-LCD is usually less than 5° and is crucial for the dark state. Therefore, an accurate measurement method to determine the pre-polar angle of a VA-R-LCD is desired.

In this section, we propose a field induced birefringence method to determine the pre-polar angle of the VA-R-LCD with low pre-polar angle. We derive theoretically the field induced optical phase retardation, which is linearly proportional to the square of the applied voltage and the pre-polar angle in the small molecular deformation regime for the small pre-polar angle. This linear relation exists not only for the reflective but also for the transmissive VA-LCD. Based on the theoretical analysis, we can determine the pretilt angle of the VA-R-LCD by measuring the phase retardation with a simple optical system. In the experiments, three liquid crystal cells were prepared. We measured the phase retardation as a function of applied voltage in two VA reflective cells and obtained the pre-polar angles from the slopes of the fitting lines in the low voltage regime. We also determined the pre-polar angle of one transmissive VA cell by this method and the result agrees well with the pre-polar angle obtained by crystal rotation technique.

3.1.1 Theory

As we know that when there is no pretilt angle on both substrates of a vertically aligned liquid crystal cell with hard boundary assumption, the tilt angles of the directors remain

zero up to the Fredericks transition threshold voltage. If the cell has nonzero pretilt angle, there is no threshold, and the phase retardation will increase as the applied voltage increases.

To obtain the relation between the phase retardation and the applied voltage, we begin with Frank's elastic free energy density under the continuum theory to calculate the director profile of LC cell under an applied voltage. We define the polar angle θ(z) as the angle from the normal direction of the cell to the LC director. The free energy per unit surface area is expressed as:

$$F = \frac{1}{2}\int_0^d \left\{ (k_{11}\sin^2\theta + k_{33}\cos^2\theta)\left(\frac{d\theta}{dz}\right)^2 + \frac{D_z^2}{\varepsilon_0(\varepsilon_{//}\cos^2\theta + \varepsilon_\perp \sin^2\theta)} \right\} dz, \qquad (3\text{-}1)$$

where D_z represents the electrical displacement in z direction, which is uniform throughout the cell, k_{11} and k_{33} are the Frank elastic constants for splay and bend deformations respectively, $\varepsilon_{//}$ and $\varepsilon_\perp$ stand for the longitudinal and transverse dielectric constants of the liquid crystals and d is the cell gap. We assume that the directors on the boundaries are fixed with the polar angle θ_0 and we call it pre-polar angle. That is, the pretilt angle is (90° – θ_0). The relation between θ(z) and the applied voltage V can be obtained by minimizing the free energy density in eq. (3-1), which is:

$$\frac{V}{V_{th}} = \frac{2}{\pi}\sqrt{(1+\gamma\sin^2\theta_m)}\int_{\theta_0}^{\theta_m}\sqrt{\frac{(1+\kappa\sin^2\theta)}{(1+\gamma\sin^2\theta)(\sin^2\theta_m - \sin^2\theta)}}d\theta, \qquad (3\text{-}2)$$

where θ_m is the polar angle of the mid-layer directors, $V_{th} = \pi\sqrt{\frac{k_{33}}{\varepsilon_0(\varepsilon_\perp - \varepsilon_{//})}}$, $\kappa = \frac{k_{11}-k_{33}}{k_{33}}$ and $\gamma = \frac{\varepsilon_\perp - \varepsilon_{//}}{\varepsilon_{//}}$.

Once we have θ(z), we can calculate the phase retardation $\Gamma(V)$ from the following equation:

$$\Gamma(V) = \frac{4\pi}{\lambda}\int_0^d \left[\frac{n_e n_o}{\sqrt{n_e^2\cos^2\theta(z) + n_o^2\sin^2\theta(z)}} - n_o \right] dz, \qquad (3\text{-}3)$$

where n_e and n_o stand for the extraordinary and ordinary refractive indices of LC material respectively, and λ is the wavelength of incident light.

In order to obtain an analytic solution, we focus our attention at low applied voltage and small deformation regime. The polar angle of the mid-layer directors can be express as

$\theta_m=\theta_0+\Delta\theta_m$, where $\theta_0>0$, and $\Delta\theta_m\geq 0$. By series expansion with respect to $\Delta\theta_m$, we have the relation between the applied voltage V and $\Delta\theta_m$:

$$\frac{V}{V_{th}}=\left(\frac{\Delta\theta_m}{\theta_0}\right)^{1/2}\left[\frac{2\sqrt{2}}{\pi}+\frac{(2+3\kappa)\sqrt{2}}{3\pi}\theta_0^2+....\right]+\left(\frac{\Delta\theta_m}{\theta_0}\right)^{3/2}\left[-\frac{5}{3\pi\sqrt{2}}+....\right]+.... \tag{3-4}$$

When $\theta_0^2 << |6/(2+3\kappa)|$ and $\Delta\theta_m/\theta_0 << 2.4$, which is deduced from $\left[\left(\frac{\Delta\theta_m}{\theta_0}\right)^{3/2}\left(\frac{5}{3\pi\sqrt{2}}\right)\right]\Big/\left[\left(\frac{\Delta\theta_m}{\theta_0}\right)^{1/2}\left(\frac{2\sqrt{2}}{\pi}\right)\right]<< 1$, Eq. (3-4) is approximately reduced to

$$\Delta\theta_m(V)=\theta_m(V)-\theta_0\approx\frac{\pi^2V^2}{8V_{th}^2}\theta_0. \tag{3-5}$$

Substitute Eq. (3-5) into $\Delta\theta_m/\theta_0 << 2.4$, and we have the limitation of the voltage: $\pi^2V^2/8V_{th}^2 << 2.4$. It means that when $V^2 << 1.95V_{th}^2$, $\Delta\theta_m$ is linearly proportional to V^2 approximately.

Similarly, we derived the relation between the phase retardation and $\Delta\theta_m$ as:

$$\begin{aligned}\Gamma(V)=\Gamma(0)+\frac{4\pi n_o d}{\lambda}\Bigg\{&\left(\frac{\Delta\theta_m}{\theta_0}\right)\left[\frac{2\nu}{3}\theta_0^2+\nu\left(\nu-\frac{4}{9}\right)\theta_0^4+....\right]\\&+\left(\frac{\Delta\theta_m}{\theta_0}\right)^2\left[\frac{11\nu}{45}\theta_0^2+...\right]+...\Bigg\},\end{aligned} \tag{3-6}$$

where $\nu=(n_e^2-n_o^2)/n_e^2$. When $\theta_0^2 << |6/(9\nu-4)|$ and $\Delta\theta_m/\theta_0 << 2.73$, which is deduced from $\left[\left(\frac{\Delta\theta_m}{\theta_0}\right)^2\left(\frac{11\nu}{45}\theta_0^2\right)\right]\Big/\left[\left(\frac{\Delta\theta_m}{\theta_0}\right)\left(\frac{2\nu}{3}\theta_0^2\right)\right]$, Eq. (3-6) is reduced to:

$$\Gamma(V)-\Gamma(0)\approx\frac{8\pi\ n_o d\,\nu}{3\lambda}\frac{\Delta\theta_m}{\theta_0}. \tag{3-7}$$

By substituting eq. (3-5) into eq. (3-7), we have

$$\Delta\Gamma(V)=\Gamma(V)-\Gamma(0)\approx\frac{\pi^3(n_e^2-n_o^2)n_o d}{3n_e^2\lambda}\frac{\theta_0^2}{V_{th}^2}V^2. \tag{3-8}$$

We analyze the limitations of the applied voltage from the range of the deformation: one is

$\Delta\theta_m/\theta_0 << 2.73$ and the other is $\Delta\theta_m/\theta_0 << 2.4$. We should choose the stricter one, which means when $V^2 << 1.95V_{th}^2$ $\Delta\Gamma$ is linearly proportional to V^2 and θ_0^2. We use the parameters of liquid crystal MLC-6608 (shown in Table. 3-I) as an example to find the applicable range. We obtained that θ_0 is less than 25° and V is less than 0.97 volts. One can use Eq. (3-8) to determine the pre-polar angles in the experiments by measuring the phase retardation.

Table 3-I Parameters used in the simulation.

Liquid crystal	MLC-6608	Cell gap	5μm
n_e	1.556	$\varepsilon_{//}$	3.6
n_o	1.4738	$\varepsilon_{\perp}$	7.8
k_{11}	11.5 pN	k_{22}	8.4 pN
k_{33}	18.1 pN	V_{th}	2.19 Volts

The merit of this method is that the phase retardation is generated by the reorientation of the directors caused by the applied voltage. The phases of other layers, such as indium/tin/oxide (ITO) and alignment layers etc., do not change when we apply a voltage to the cell, therefore, they do not influence the results. Beside, we can use the same optical setup to obtain the cell gap. That is the phase retardation $\Gamma(V)$ in the high voltage regime can be written as [12-14]:

$$\Gamma(V) = \frac{4\pi(n_e - n_o)\,d}{\lambda}\left(1 - \zeta\frac{V_{th}}{V}\right), \tag{3-9}$$

where ζ is a material constant. When $V\to\infty$, all the directors are reoriented by the field and the maximum phase retardation $\Gamma_{\max} = 4\pi(n_e - n_o)d/\lambda$ is achieved. Therefore, we use the extrapolation method to get the maximum phase retardation and the cell gap can be derived from it [12].

In one word, we have designed a field induced birefringence method to determine the pre-polar angle by simply measuring the phase retardations with respect to the applied voltages. We get the cell gap by extrapolating the curve of the phase retardations versus the inverse of the applied voltage in the high voltage regime. By using this cell gap, we determine the pre-polar angle from the slope of the linear part of the phase retardation versus the square of the applied voltage in the low voltage regime.

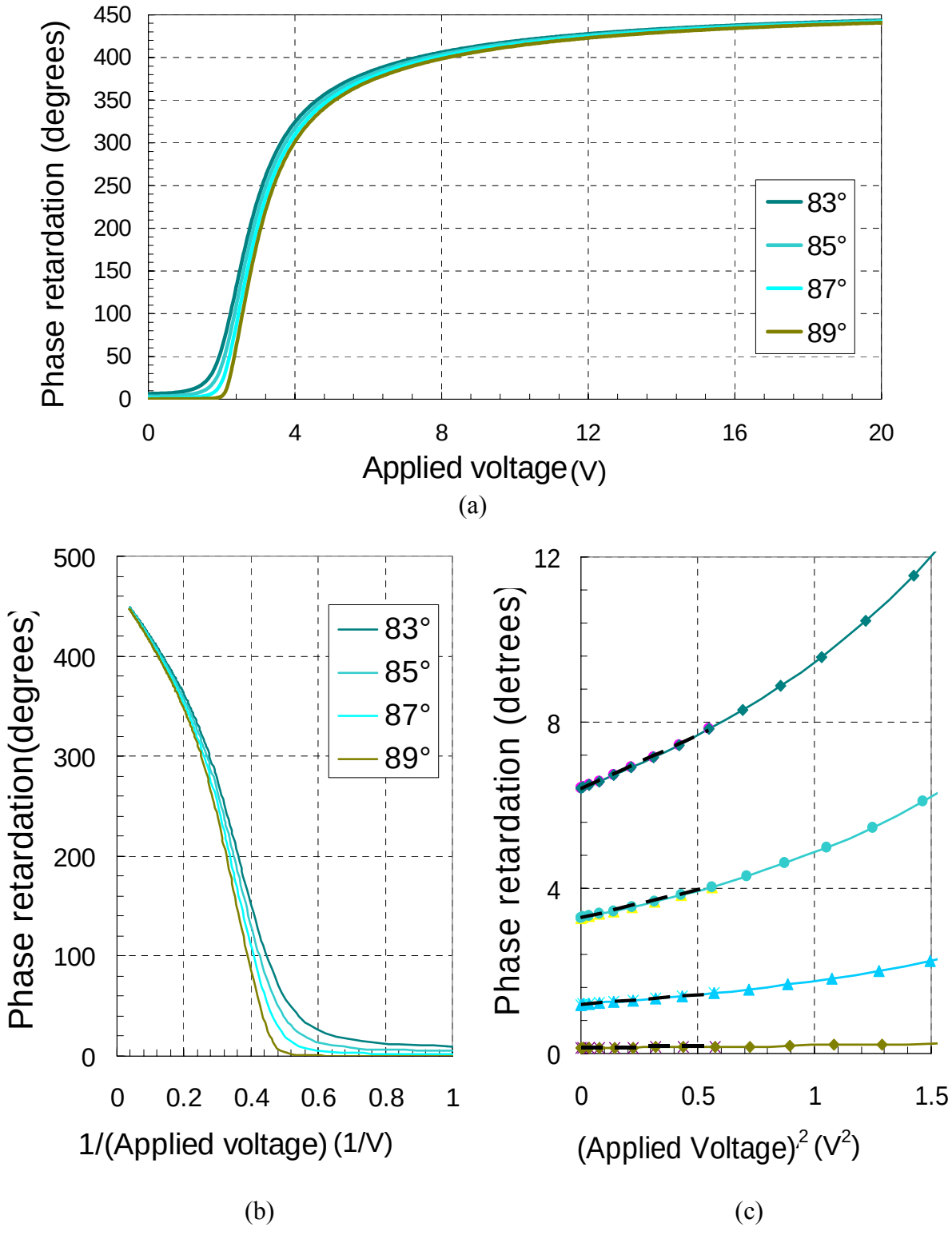

Figure 3.1 The phase retardations obtained from the simulated director profiles for pre-polar angle from 1° to 7°: (a) with respect to the applied voltage, (b) with respect to the inverse of the applied voltage, (c) with respect to the square of the applied voltage. The linearly fitting curves are plotted in dash lines for each pre-polar angles.

Table 3-II The pre-polar angles obtain in the Figure 3.1(c) with different fitting ranges of the square of the applied voltage. The upper limit of the applied voltage is V_{upper} and θ_{0s} and θ_{0e} are the pre-polar angles used in the simulation and calculated from the slopes in Figure 3.1(c), respectively.

θ_{0e} \ V_{upper}^2 / θ_{0s}	0.2 (volts^2)	0.3 (volts^2)	0.4 (volts^2)	0.5 (volts^2)
1°	1.029	1.047	1.062	1.076
3°	3.082	3.128	3.164	3.211
5°	5.089	5.187	5.260	5.332
7°	7.159	7.234	7.321	7.420
9°	9.168	9.259	9.358	9.479
Error (%)	< 2.9%	< 4.7%	< 6.5%	< 7.7%

In order to illuminate this idea, we use the commercial simulator DIMOS to obtain the director profile of the LC cell with varied pre-polar angles and applied voltages. Table 3-I shows the parameters of the liquid crystal used in this simulation. We accumulate the phase retardation layer by layer and plot them in Figure 3.1(a). To calculate the cell gap, we re-plot the phase retardations versus the inverse of the applied voltage and the results are shown in Figure 3.1(b). We derive the maximum phase retardations and the corresponding cell gaps from the intercept of the extrapolation lines in the high voltage regime. Figure 3.1(c) shows the phase retardations versus the square of the applied voltages. The dash lines are linear fitting curves. We calculate the pre-polar angles with Eq. (3-7) by using the slopes of the fitting lines in the different applied voltage ranges and the results are in Table II. Theoretically, the smaller the fitting voltage range, the more accurate the fitting pre-polar angles will be. However, the experimental data fluctuate and contain errors, so it is inappropriate to have too small voltage range for fitting. Table 3-II shows the calculated pre-polar angle and corresponding errors by using this method.

3.1.2 Experimental results and comparisons

With the proposed method, we measured two VA reflective cells and one transmissive VA cell in the small pre-polar angle range. Figure 3.2 shows a schematic diagram of our reflective phase retardation measurement setup.

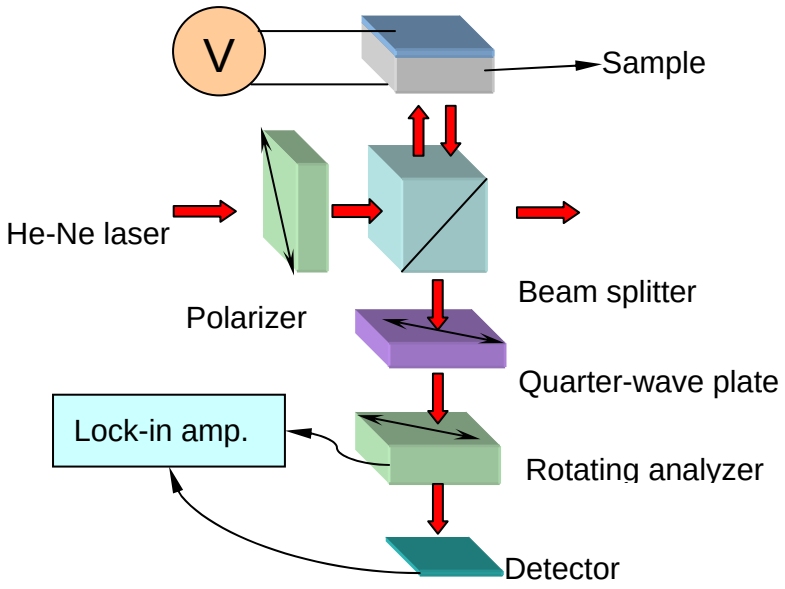

Figure 3.2 The optical setup used for measuring the phase retardation of a reflective VA-LC cell.

The light from a He-Ne laser (0.6328 μm) passes through the linear polarizer and beam splitter, then impinges on the LC cell with the polarization at an angle of 45° to the rubbing direction. The ordinary and extraordinary waves experience different phases in the LC cell and the light is reflected and leaves the cell with elliptical polarization. Then it passes through the beam splitter again and a quarter wave plate, which is in the same alignment with the input polarizer. The light is transferred to the linearly polarized light and goes through a rotating analyzer, then hits on the optical detector. The lock-in amplifier analyzes the signals and the output phase retardations are delivered to the computer, which is programmed to average the row data in order to raise the accuracy. By changing the voltage applied on the cell, we have the phase retardation as a function of applied voltage.

We used two ITO coated glasses, one of which was with aluminum under ITO as a reflector, to fabricate one VA reflective cell. With the polymer JALS-2021 as the homeotropic alignment layers, we used rubbing method to produce pretilt angle. We combined the substrates by using 4μm-spacers mixed in the adhesive without spread in the cell. Then filled it with liquid crystal MLC-6608. The measured phase retardation is shown in Figure 3.3(a), the relation between the measured phase retardation and the inverse of the applied voltage is shown in Figure 3.3(b). From the intercept of the extrapolation, the maximun phase retardation is 328° and the calculated cell gap is 3.51 μm. In order to get the pre-polar angle, we re-plot the phase retardations versus the square of the voltage

again as shown in Figure 3.3(c). From the slope of the linearly fitting curve, the pre-polar angle of the cell is 4.3°.

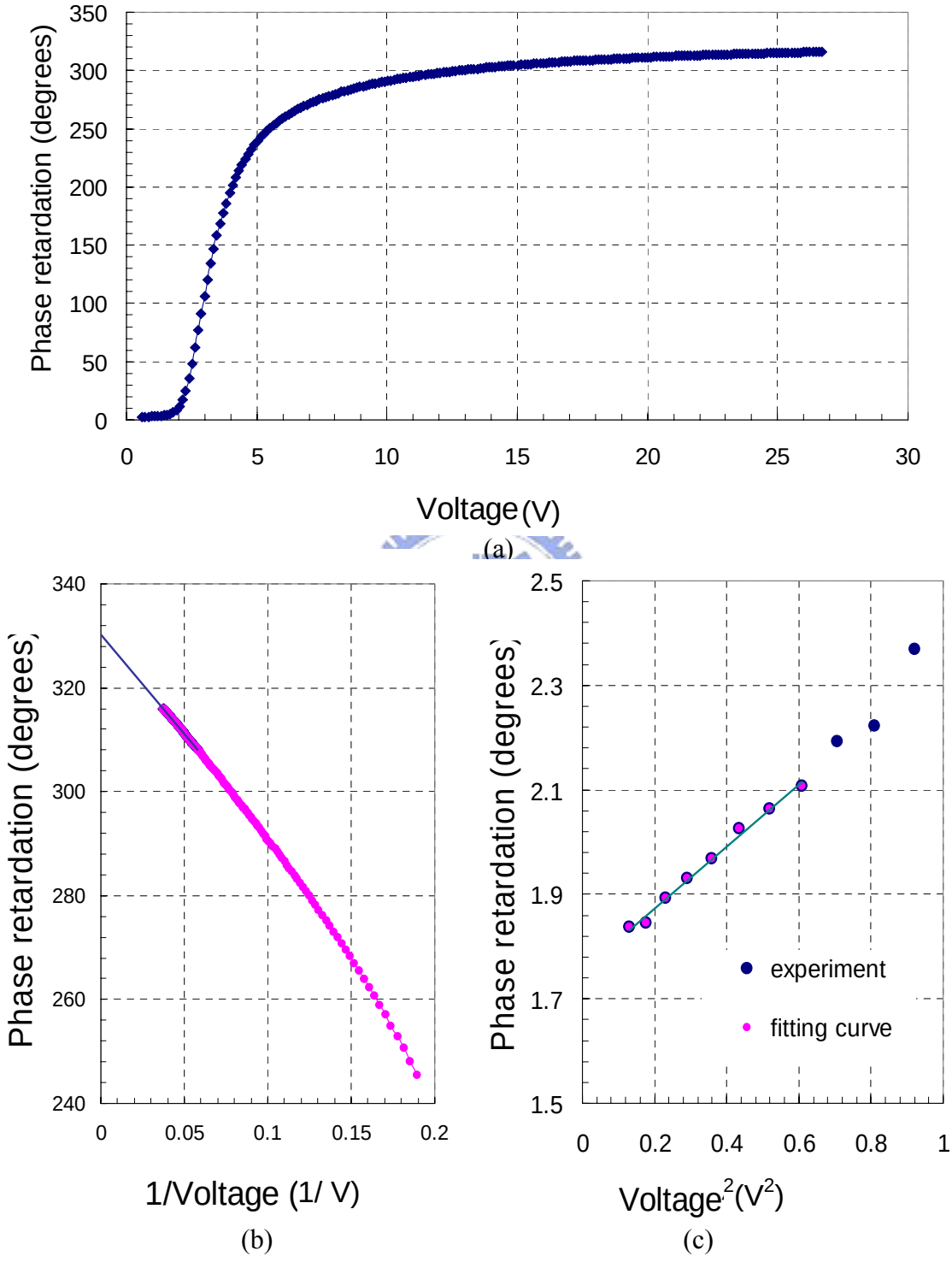

Figure 3.3 The measured phase retardation of the VA reflective cell: (a) with respect to the applied voltage, (b) with respect to the inverse of the applied voltage, (c) with respect to the square of the applied voltage. The solid lines in (b) and (c) are the linearly fitting curves to get the cell gap and the pre-polar angle, respectively.

The other VA reflective cell was provided by ERSO/ITRI of which the manufacture processes are similar to that of the LCD factory. The 4μm-spacers were spread uniformly in the cell, and then filled with liquid crystal MJ011675. By using the proposed method, we obtain the cell gap and the pre-polar angle to be 3.89μm and 0.8° respectively.

To verify the reliability of the above theory, we fabricated a transmissive cell since our theory is applicable for it. Besides, we can confirm the pre-polar angle of the cell by the conventional crystal rotation method [(2)]. However, the He-Ne laser passes through the transmissive cell only once instead of twice, we modify Eq. (3-8) to

$$\Delta\Gamma(V) \approx \frac{\pi^3 (n_e^2 - n_o^2) n_o d}{6 n_e^2 \lambda} \frac{\theta_0^2}{V_{th}^2} V^2. \qquad (3\text{-}10)$$

The cell gap is determined to be 11.26μm and the pre-polar angle is 3.98° when the fitting range is 0 ~ 0.5 volts^2. The pre-polar angle measured by the crystal rotation method is 3.99° which agrees excellently with the one obtained by our field induced birefringence method.

3.1.3 Conclusion

We have proposed a simple method to determine the pre-polar angle of a non-twisted homeotropic LC cell with negative anisotropic nematic liquid crystals, which the conventional measurement methods are not applicable. A simple equation is deduced from the relationship between the pre-polar angle and the phase retardation as a function of applied voltage. In the experiments, we have applied this method and determined the pre-polar angles of two reflective VA cells. We also compared the method with the crystal rotation method by measuring one transmissive VA cell and the result is satisfactory. This method enables us to monitor the reflective VA cell in the manufacture, aging, and stability processes, which is important for the study of the liquid crystal displays.

3.2 Determination of the higher order polar anchoring coefficients

Once we know the coordinate of the easy axis, we can study the surface anchoring energy density in the polar direction. We extend the Rapini-Papoular (RP) model with one higher order term for the non-twisted LC cells and propose a method to determine the coefficients of the modified surface anchoring energy density. By analyzing the measured phase retardations as a function of applied voltage with the simulated curves, we determine the surface anchoring energy density of 2 homogeneous and 3 homeotropic cells.

3.2.1 Theory

Since the director distortions calculated from the RP model do not agree well with the observations in strong external fields, we adopt the Lagendre polynomials which are derived from the spherical-harmonic expansion and keep one more term in addition to the RP model. Due to the equivalence of $\vec{n}$ and $-\vec{n}$, the odd-order terms disappear. The modified anchoring energy density, f_{sm}, can be expressed as:

$$f_s \approx f_{sm} = \frac{1}{2} W_{\theta,m} \sin^2(\alpha_s - \alpha_0)[1 + \zeta \sin^2(\alpha_s - \alpha_0)], \qquad (3\text{-}11)$$

where ζ is a parameter of the higher order term for modifying the RP model and $W_{\theta,m}$ is the anchoring energy coefficient of the modified model. We use Eq. (3-11) as the surface free energy density to analysis the configuration of the directors. Comparing with that derived from RP model, we use the slight differences between them to determine ζ.

Consider a homogeneous nematic LC layer confined between the planes $z = -d/2$ and $z = d/2$, as shown in Figure 3.4. The two boundaries are treated in the same way and anti-parallel aligned. When there is no applied field, all directors are oriented to the pretilt angle α_0 from the x-axis, which is the tilt angle of the easy axis on the substrate. When the applied electric field increases, the tilt angle of the director at the boundary deviates from the easy axis due to finite surface free energy. The tilt angle of the middle layer director α_m achieves maximum and satisfies $\left.\frac{d\alpha}{dz}\right|_{z=0} = 0$.

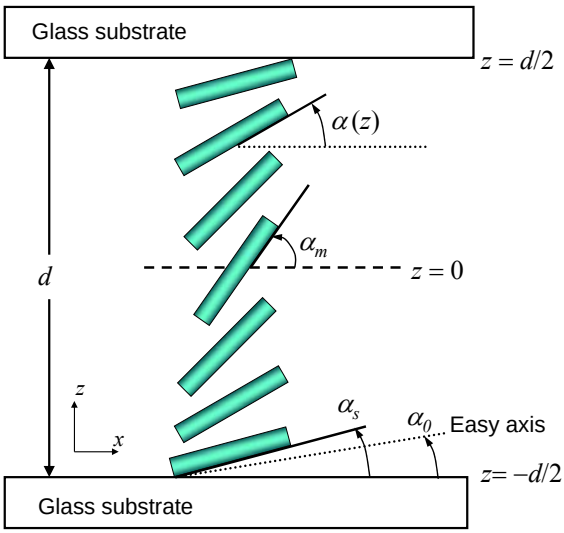

Figure 3.4 Sketch of geometry and coordinates for a homogeneous nematic layer deformed by an applied field.

On the basis of the elastic continuum theory, the stable liquid crystal configuration with the tilt angle $\alpha(z)$ for any given field can be derived by minimizing the free energy per unit area of the system, which is the sum of the volume and surface contribution, and is expressed as:

$$f_{total} = \int_{-d/2}^{d/2} \left[(k_{11}\cos^2\alpha + k_{33}\sin^2\alpha)\left(\frac{d\alpha}{dz}\right)^2 - \vec{D}\cdot\vec{E} \right] dz + f_s\big|_{z=-d/2} + f_s\big|_{z=d/2}, \qquad (3\text{-}12)$$

where k_{11} and k_{33} are the splay and bend elastic constants, respectively. $\vec{D}$ is the electric displacement, $\vec{E}$ is the applied electric field and $E_z = \dfrac{D_z}{[\varepsilon_\perp \cos^2\alpha + \varepsilon_{//}\sin^2\alpha]}$, with α being the angle between $\vec{n}(z)$ and the x axis. $f_s\big|_{z=d/2}$ and $f_s\big|_{z=-d/2}$ are the surface free energies per unit area of the substrates.

Applying the calculus of variations to minimize the free energy of the system leads to the following three equations that describe the equilibrium deformation: the bulk equation:

$$(k_{11}\cos^2\alpha + k_{33}\sin^2\alpha)\frac{d^2\alpha}{dz^2} + (k_{33}-k_{11})\sin\alpha\cos\alpha\left(\frac{d\alpha}{dz}\right)^2 + \frac{D_z^2\Delta\varepsilon\sin\alpha\cos\alpha}{\varepsilon_0(\varepsilon_{//}\sin^2\alpha + \varepsilon_\perp\cos^2\alpha)} = 0, \qquad (3\text{-}13)$$

And two boundary conditions that are the torque balance equations at $z = -d/2$ and $z = d/2$, that is,

$$[k_{11}\cos^2(\alpha_s)+k_{33}\sin^2(\alpha_s)]\frac{d\alpha}{dz}\bigg|_{z=d/2}=\frac{df_s}{d\alpha}\bigg|_{z=d/2}, \tag{3-14}$$

$$[k_{11}\cos^2(\alpha_s)+k_{33}\sin^2(\alpha_s)]\frac{d\alpha}{dz}\bigg|_{z=-d/2}=-\frac{df_s}{d\alpha}\bigg|_{z=-d/2}. \tag{3-15}$$

After manipulation, we obtain the following equation in $0<z<d/2$ due to the symmetry of the cell:

$$\frac{d\alpha}{dz}=\frac{D_z}{\varepsilon_0\varepsilon_\perp}\sqrt{\frac{(\varepsilon_{//}-\varepsilon_\perp)(\sin^2\alpha_m-\sin^2\alpha)}{k_{11}(1+\kappa\sin^2\alpha)(1+\gamma\sin^2\alpha)}}. \tag{3-16}$$

We also obtain the boundary condition if we use RP model:

$$[k_{11}\cos^2\alpha_s+k_{33}\sin^2\alpha_s]\frac{d\alpha}{dz}\bigg|_{z=d/2}=\frac{df_{RP}}{d\alpha}\bigg|_{z=d/2}=W_{\theta,RP}\sin(2\Delta\alpha). \tag{3-17}$$

When we use the modified model, we obtain another boundary condition:

$$[k_{11}\cos^2\alpha_s+k_{33}\sin^2\alpha_s]\frac{d\alpha}{dz}\bigg|_{z=d/2}=\frac{df_{sm}}{d\alpha}\bigg|_{z=d/2}=W_{\theta,m}\sin(2\Delta\alpha)(1+2\zeta\sin^2\Delta\alpha). \tag{3-18}$$

Once we have the configuration of $\alpha(z)$, the phase retardation δ of the non-twisted cell can be calculated from:

$$\delta=\frac{2\pi}{\lambda}\int_0^d\left[\frac{n_e n_o}{\sqrt{n_e^2\sin^2\alpha(z)-n_o^2\cos^2\alpha(z)}}-n_o\right]dz. \tag{3-19}$$

When the applied voltage is small, $\Delta\alpha$ is small. The higher order term of Eq. (3-11) has little effect on Eq. (3-18). For $W_{\theta,m}$ = $W_{\theta,RP}$, the derived $\alpha(z)$ is the same for these two models and the δ–V curves overlap. Accordingly, we determine $W_{\theta,m}$ as $W_{\theta,RP}$ from a small applied voltage regime[15].

As we increase the applied voltage, $\Delta\alpha$ is enlarged. Since the higher order term cannot be neglected in Eq. (3-18), the derived α_s's from these two models are different gradually and the δ–V curves are apart as the applied voltage increases. In the large applied voltage regime ($V>10V_{th}$), most of the directors are vertical (α_m = 90°) except those near the boundaries, thus the contribution of phase retardation mainly comes from the layers near the boundaries. If ζ of the homogeneous cell is positive, from Eqs. (3-17) and (3-18) the surface torque induced by the anchoring energy density is larger in the modified model for the same $\Delta\alpha$. In other words, the calculated $\Delta\alpha$ and α_s are smaller for the

modified model than for the of RP model under the same applied voltage. Therefore, the δ–V curve of the modified model decreases slowly as the applied voltage increases and crosses with the δ–V curves of different $W_{\theta,RP}$ value calculated using the RP model. For these crossed points, in which the phase retardation and the applied voltage are the same, we consider that the derived α_s's are identical for these two models. Substituting α_s into Eq. (3-16), we derive the same $d\alpha/dz\big|_{z=d/2}$ for the modified and PR models. Then, from Eqs. (3-17) and (3-18), we have the following equations at the crossed points:

$$\begin{aligned}[k_{11}\cos^2(\alpha_s)+k_{33}\sin^2(\alpha_s)]\frac{d\alpha}{dz}(\alpha_s) &= \left.\frac{df_{RP}}{d\alpha}\right|_{z=d/2} = W_{\theta,RP}\sin(2\Delta\alpha),\\ &= \left.\frac{df_{sm}}{d\alpha}\right|_{z=d/2} = W_{\theta,m}\sin(2\Delta\alpha)(1+2\zeta\sin^2\Delta\alpha).\end{aligned} \tag{3-20}$$

ζ can be derived by

$$\zeta = \frac{W_{\theta,m}-W_{\theta,RP}}{2W_{\theta,m}\sin^2(\Delta\alpha)}. \tag{3-21}$$

Therefore, we can determine ζ through the crossed points in this regime ($V>10V_{th}$).

3.2.2 Experiment

The voltage dependence of the phase retardation δ was measured in a setup shown in Figure 3.5. The light from a He-Ne laser (0.6328 μm) passes through the linear polarizer and impinges on the LC cell with polarization at an angle of 45° to the rubbing direction. The ordinary and extraordinary waves experience different phases in the LC cell. The light leaves the cell with elliptical polarization. Then it passes through a quarter wave plate, which is in the same alignment with the input polarizer. The light is transferred to the linearly polarized light and goes through a rotating analyzer, then hits on the optical detector. The lock-in amplifier analyzes the signals and outputs phase retardations to the computer, which is programmed to average the row data in order to increase the accuracy. By changing the voltage applied on the cell, we obtain the phase retardation as a function of applied voltage.

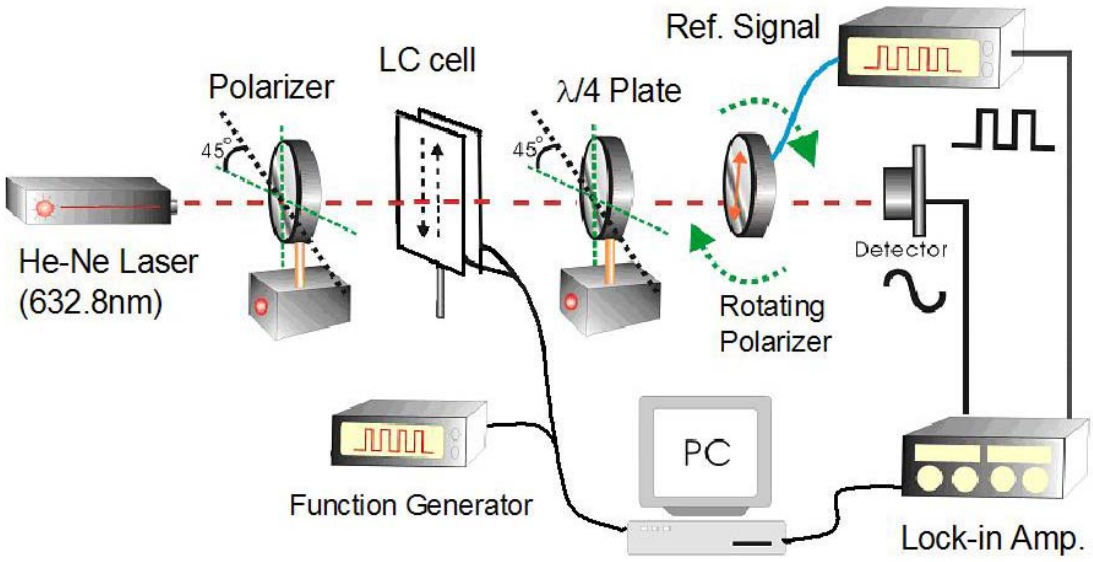

Figure 3.5 The setup for measuring the phase retardation as a function of applied voltage.

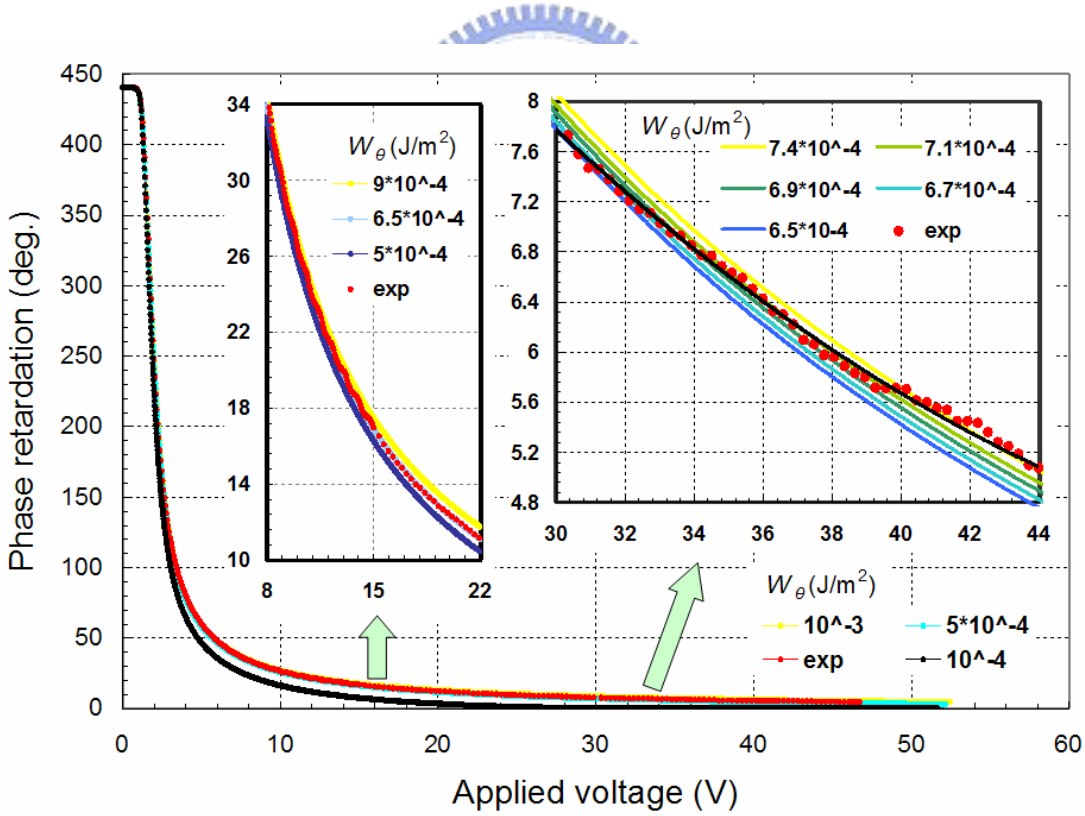

Figure 3.6 The measured δ–V curve together with a series of δ–V curves simulated with different $W_{\theta,RP}$ of a homogeneous cell. The left inset shows the small applied voltage regime in which the experimental δ–V curve agrees well with one of the simulated curves. The right inset shows δ–V curves in the large applied voltage regime in which the experimental curve is intercepted with simulated curves of different $W_{\theta,RP}$.

By comparing δ–V curve in the low applied field regime to the simulated curves from the commercial simulator DIMOS, we can determine $W_{\theta,m}$. Then, use the equation of ζ derived theoretically for the crossed points of δ–V curve and the simulated curves, we can calculate ζ. With this method, we have measured two homogeneous and three homeotropic cells with different alignment layers and liquid crystals.

The measured δ–V curve together with a series of δ–V curves simulated using the different $W_{\theta,RP}$ values of a homogeneous cell is shown in Figure 3.6 as an example. The simulated curves were obtained by accumulating the phase retardation layer by layer in which the directors are calculated from the commercial simulator DIMOS. The experimental curve is laid between the simulated curves of $W_{\theta,RP} = 5.0\times10^{-4}$ and 1.0×10^{-3} J/m^2; however, these three curves almost overlap in Fig.3.6. Therefore, we magnified them under an applied voltage of 22 V in the left inset and simulated more curves with different $W_{\theta,RP}$ values. To obtain a clear figure, we did not show all the simulated curves in the left inset. Finally, the experimental curve and the simulated curves with $W_{\theta,RP} = 6.5\times10^{-4}$ J/m^2 match well in this regime. Therefore, we chose $W_{\theta,m} = 6.5\times10^{-4}$ J/m for this LC cell.

However, as the applied voltage increased we simulated more curves with different $W_{\theta,RP}$ values, which are shown in the right inset of Figure 3.6. The black line is the fitting curve of the experimental data that decreases more slowly than the simulated curves of $W_{\theta,RP} = 6.5\times10^{-4}$ J/m. It gradually passes the simulated curves of $W_{\theta,RP} = 6.7\times10^{-4}$, 6.9×10^{-4}, 7.1×10^{-4}, 7.3×10^{-4} and 7.4×10^{-4} J/m. We obtained these crossed points, calculated ζ using Eq. (3-21) and averaged them to have ζ=0.51 for this cell.

3.2.3 Discussion and Conclusion

We measured the δ values of two homogeneous cells and three homeotropic cells. The determined $W_{\theta,m}$ and ζ together with the corresponding cell parameters, alignment materials and methods are listed in Table 3-III. For the material used in our experiments, we find that the $W_{\theta,m}$ values of the homogeneous alignment are higher than that of the homeotropic alignment and that the rubbing alignment method achieves larger $W_{\theta,m}$ values than the photo alignment method. As for ζ, even with a different PI and alignment method, we obtained a positive value for the homogeneous cells and negative for the homeotropic cells.

Figure 3-7 shows the surface anchoring energy density F_s as a function of $\Delta\alpha$ for the homogeneous cell A and homeotropic cell C in Table 3-III, where $f_{RP} = \frac{1}{2} W_{\theta,m} \sin^2(\Delta\alpha)$, and $f_{sm} = \frac{1}{2} W_{\theta,m} \sin^2(\Delta\alpha)[1 + \zeta \sin^2(\Delta\alpha)]$. The walls of homogeneous cell A are obviously higher than that of the homeotropic cell C. For cell A with a positive ζ value, f_{sm} is steeper than f_{sm} at the large $\Delta\alpha$ regime, as shown in the first line from the left in Figure 3.7. This indicates that the directors at the boundaries are more difficult or require more energy to pull further away from the substrate than the case predicted using the PR model. For cell C with a negative ζ value, f_{sm} is flatter as shown in the last line from the left of Figure 3.7. This indicate that the directors at the boundaries are easier to tilt toward the substrate. A negative ζ value was also obtained by Yang[16] with a magnetic field for a homeotropic cell. These results confirm that our proposed method of determining higher order polar anchoring energy coefficients is applicable.

Table 3-III. The determined W_θ, ζ and the corresponding alignment materials, the methods, cells parameters.

Cell	A	B	C	D	E
LC material	MJ01744		MLC-6882		
Alignment	Homogeneous		Homeotropic		
Alignment material	PI -A	PI-B	DMOAP	JSR-2021	JSR-2021
Alignment method	Rubbing	Photo	Rubbing	Rubbing	Photo
Pretilt angle	2.22°	0.08°	89.55°	89.5°	89.72°
Thickness (μm)	8.72	10.23	6.09	8.47	6.9
W_θ (10^{-4} J/m^2)	6.5	5.0	1.6	2	0.75
ζ	0.51	1.33	-0.31	-1.67	-0.22

On the basis of the elastic continuum theory of a nematic LC and the modified model for the surface anchoring energy density, we obtained the coefficient of the higher order term in the modified model through the measured optical phase retardations. From our experiments, we find that when the deviation angle ($\Delta\alpha$) is large the higher order term of

the surface free energy is marked. Therefore, we should be very careful in using HEF method for measuring the polar anchoring energy coefficient because weak anchoring may have a large $\Delta\alpha$ value at a moderate applied voltage. If this occurs, the PR model is unsuitable for the HEF method, so the derived polar anchoring energy coefficient is incorrect.

It is very interesting to obtain ζ values with opposite signs for the homogeneous and homeotropic alignment cells. Further investigations are required to determine the relationship between the LC, alignment and the anchoring energy coefficients.

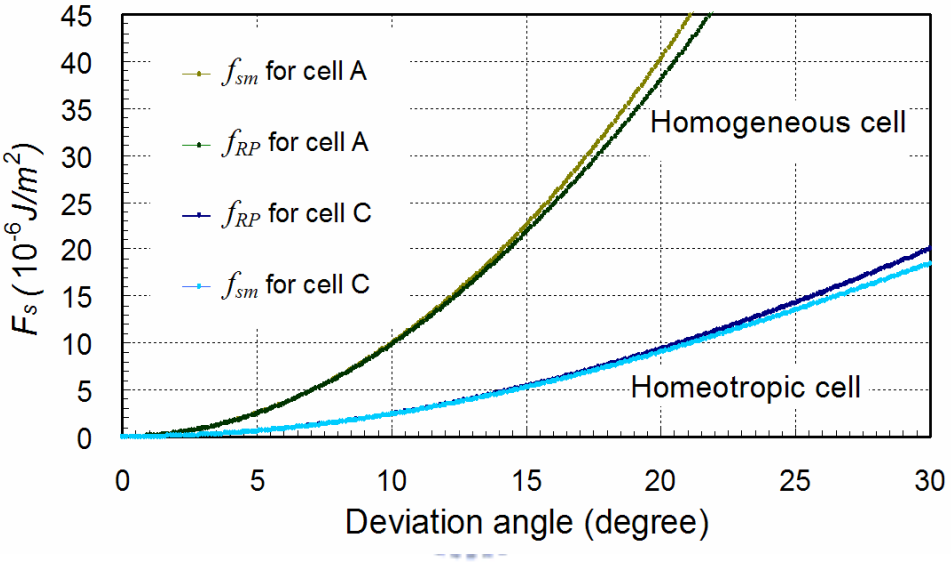

Figure 3.7 The anchoring energy versus the deviation angle of (a) a homogeneous cell, (b) a homeotropic cell.

References of Chapter 3

[1] T. J. Scheffer and J. Nehring, *J. Appl. Phys.*, **48**, 5, 1783, (1977).

[2] G.Baur, V. Wittwer and D. W. Berreman, *Physics Lett. A*., **56**, 2, 142-4, (1976).

[3] Jin Seog Gwag etc., *J. Appl. Phys.*, **93**, 8, 4936, (2003).

[4] K. Y. Han, T. Uchida and S. B. Kwon, *Mol. Cryst. Liq. Cryst.,* **302**, 1145-50, (1997).

[5] G. P. Sinha, Bs. Wen, and C. Rosenblatt, *Appl. Phys. Lett.,* **79**, 16, 2543, (2001).

[6] H. Yokoyama and H. A. van Sprang, J. Appl. Phys. **57**, 4520, (1985).

[7] H. Yokoyama and R. Sun, Jpn. J. Appl. Phys. **39**, L45, (2000).

[8] Yu. A. Nastishin, R. D. Polak, S. V. Shiyanovskii, V. H. Bodnar, and O. D. Lavrentovich, J. Appl. Phys. **86**, 4199, (1999).

[9] Xinyu Zhu, Wing-Kit Choi, and Shin-Tson Wu, *IEEE Trans. Electron Devices*, **45**, 11, 1863, (2002).

[10] S. T. Tang, and H. S. Kwok, J. Appl. Phys. **91**, 11, 8950, (2002).

[11] Shin-Tson Wu, and Ganf Xu, *IEEE Trans. Electron Devices*, **47**, 12, 2290, (2000).

[12] Shu-Chan Hsiao, Jy-Shan Hsu, Bau-Jy Liang and Shu-Hsia Chen, Journal of SID, **11**, 4, 629, (2003).

[13] Iam-Choon Khoo, and Shin-Tson Wu, "Optics and nonlinear optics of liquid crystals", World Scientific Publishing Co. Pte. Ltd, 153, (1993).

[14] Shin-Tson Wu, and Chiung- Sheng Wu, *Appl. Phys. Lett.,* **53**, 19, 1794, (1988).

[15] M. C. Hsieh, B. J. Liang, C. L. Yang and S. H. Chen, Taiwan Display Conference Proceeding, 172, (2004).

[16] K. H. Yang, J. Appl. Phys. **53**, 6742, (1982).

Chapter 4

Bistable nematic liquid crystal cells (BiNem)

4.1 Introduction

Bistable displays have received considerable attention recently because the power consumption can be reduced by their two (or more) stable states. Among them, the bistable twisted nematic liquid crystal cell (2π-BTN) [1,2] has excellent contrast and brightness. Its two states can be switched by controlling the shear flow effect. However, the lifetimes of these states are not very long because a more stable intermediate state exists. To solve this problem, Dozov *et al.* [3] proposed a bistable nematic liquid crystal cell (BiNem) which has a permanent memory effect. The two stable states, the twisted angles of which differ by π, can be switched through the shear flow effects and polar anchoring energy breaking on one substrate. The theoretical investigations of the switching mechanisms have been studied by Dozov and Durand. [4] The influences of the azimuthal anchoring energy on the stable states have been analyzed by Saito *et al.* [5] When Takahashi *et al.* [6] used a computer to simulate the dynamic behaviors of the BiNem cells, they found that the director configuration switched from the U state to the T state takes a 270° twist first, and then gradually changes to the T state. This behavior is different from that of the model proposed by Dozov, in which the directors switch directly to the T state.

In the next section, we investigate the transient behaviors of the BiNem cell using the commercial simulator DIMOS. Different dynamic behaviors appear when we apply the pulses of 13 V with different durations to a U-state cell. One, which is the relaxation process of the 2 ms pulse, agrees well with the model proposed by Dozov, and we call it the

normal-twisted relaxation process. The other is similar to the results simulated by Takahashi, and we call it the over-twisted relaxation process. The relaxation time of the over-twisted relaxation process is 1.5 times that of the normal-twisted relaxation process. If we further reduce the duration of the pulse to 0.5 ms, the cell cannot be switched to the T state. The mechanisms of the different behaviors are explicitly explained through the tilt and azimuthal angles of the director on the weak anchoring boundary in the dynamic process.

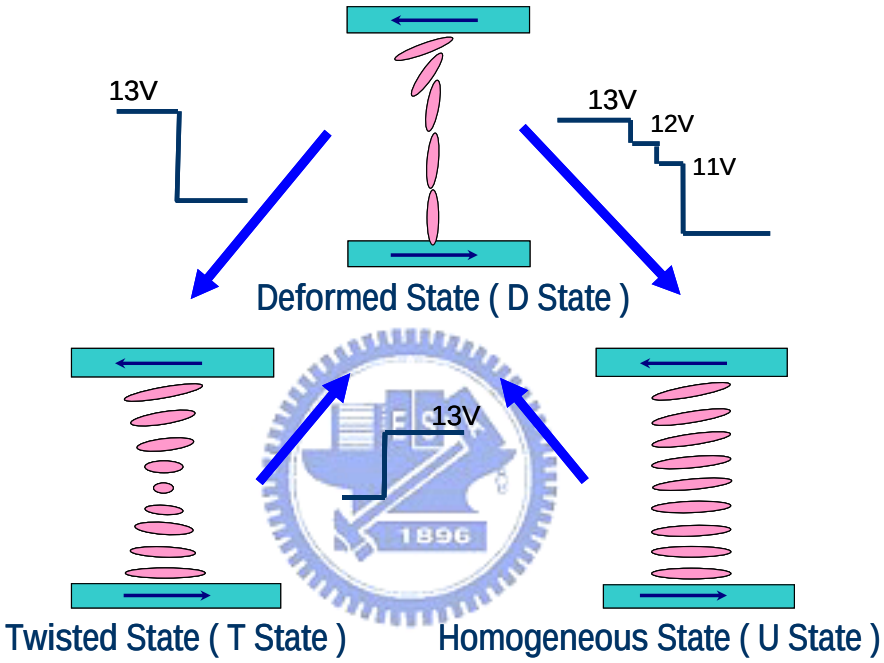

Figure. 4.1 The textures and the transitions of the BiNem cell.

4.2 Dynamic behaviors induced by pulses with different durations

According to the papers of Dozov, the two stable states of the BiNem cell are the U state and the T state. The upper substrate is treated to have strong polar anchoring energy with large pretilt angle, and the bottom substrate has weak polar anchoring energy and a pretilt angle of nearly zero. The textures and transitions of these states are shown in Figure 4.1. By applying a moderate electric field in the vertical direction, the bulk directors are nearly homeotropic, and parallel to the field. However, the directors on the boundaries, which are influenced by the surface anchoring torque, are tilted in the rubbing

direction. If the field is larger than the critical electric field, which is defined as the anchoring energy breaking of the bottom substrate, the directors near the bottom substrate are vertical (D state in Figure 4.1). After the field is removed, the directors relax to either one of the bistable states. According to the theory proposed by Dozov, the final state selection is determined by the flow effect induced by the pulse. Rapidly switching off the field creates a strong shear flow, and the cell relaxes to the T state. Slowly switching off the field does not induce enough shear flow, and the cell goes back to the U state.

Table 4-I The cell and liquid crystal material parameters used in the simulation.

Cell gap	3 μm	Pitch	16 μm
Wavelength	550 nm	k_{11}	12.5 pN
		k_{22}	7.5 pN
Top boundary :		k_{33}	17.9 pN
Pretilt angle	5°	$\varepsilon_{//}$	14.1
$W_{\theta t}$	1.3×10^{-3} J/m^2	$\varepsilon_{\perp}$	4.1
$W_{\phi t}$	1.3×10^{-4} J/m^2	n_o	1.499
		n_e	1.631
Bottom boundary :		γ_1	0.153 Pa·s
Pretilt angle	0.1°	η_1	0.185 Pa·s
$W_{\theta b}$	1.4×10^{-4} J/m^2	η_2	0.0308 Pa·s
$W_{\phi b}$	1.4×10^{-5} J/m^2	η_3	0.055 Pa·s
		η_{12}	-0.0216 Pa·s

We use DIMOS to simulate the dynamic behavior of the transition process from the U state. The Oseen-Frank expressions are adopted for the bulk elastic free energy and the Ericksen-Leslie equations in one dimension are used in the dynamic calculation. The anchoring energy density of the substrate is given by [7]

$$f_s = \frac{1}{2}W_\theta \sin^2(\alpha-\alpha_e) + \frac{1}{2}W_\phi \sin^2(\phi-\phi_e)\cos^2\alpha, \qquad (4\text{-}1)$$

where α_e and ϕ_e are the tilt (from the substrate) and azimuthal angles of the easy axis on the boundary, α and ϕ are the tilt and azimuthal angles of the director on the boundary, and W_θ and W_ϕ are the polar and azimuthal anchoring energy coefficients, respectively. This

equation is based on the Rapini-Papoular approach extended to include weak azimuthal coupling [7].

In our simulation, we apply two pulses of 13 V with durations of 2 ms and 1 ms to the U state cell. The polar anchoring energy coefficient of the upper boundary is 1.3×10^{-3} J/m^2, and that of the bottom boundary is 1.4×10^{-4} J/m^2. The azimuthal anchoring energy coefficients are one-tenth of the polar anchoring energy coefficients. The rubbing directions are on the *x*-axis and are antiparalleled. The pretilt angles are 5° and 0.1° on the top and bottom boundaries, respectively. The cell gap is 3 μm. The liquid crystal material parameters are shown in Table 4-I.

By applying a 2 ms pulse to the U state cell, the directors are pulled first to the deformed state. When the field is off, the director on the bottom boundary ($\vec{n}_b$) reorients directly toward the –*x* direction, and the cell relaxes to the T state. This normal-twisted relaxation process of the directors is shown in Figure 4.2(a). Each line in the diagram is the trajectory of the directors from the bottom to the top layers projected on the *x*-*y* plane. With a polarizer parallel to the *x*-axis and crossed to an analyzer, the transmittance of the cell rises monotonically and the response time is about 27 ms as shown in Figure 4.2(b). On the other hand, when the voltage from a 1 ms pulse is off, the directors of the cell are over-twisted first and then gradually relax to the T state. This over-twisted relaxation process of the directors is shown in Figure 4.3(a). There is a bump in the transmittance, and the relaxation time is around 41 ms as shown in Figure. 3(b).

4.3 Analysis

In order to analyze the mechanisms of these dynamic behaviors in the relaxation processes, we derive the polar anchoring torque from Eq. (3-1) as

$$\frac{\partial f_s}{\partial \alpha} = \frac{1}{2} W_\theta \sin[2(\alpha - \alpha_e)] - \frac{1}{2} W_\phi \sin^2(\phi - \phi_e) \sin(2\alpha). \qquad (4\text{-}2)$$

In our simulation with $\alpha_e = 0.1°$ in the bottom boundary, when the tilt angle of $\vec{n}_b$ is nearly 90° ($\alpha_b \approx 90°$), the polar anchoring torque ($\partial f_s / \partial \alpha$) acting on $\vec{n}_b$ is almost zero. As α_b decreases from 90°, the polar anchoring torque increases. To investigate the behavior of $\vec{n}_b$, we plot the tilt and azimuthal angles (ϕ_b) of $\vec{n}_b$ as we apply 2, 1, and 0.5 ms pulses of 13 V to a U-state cell, shown in Figures 4.4(a), (b) and (c), respectively.

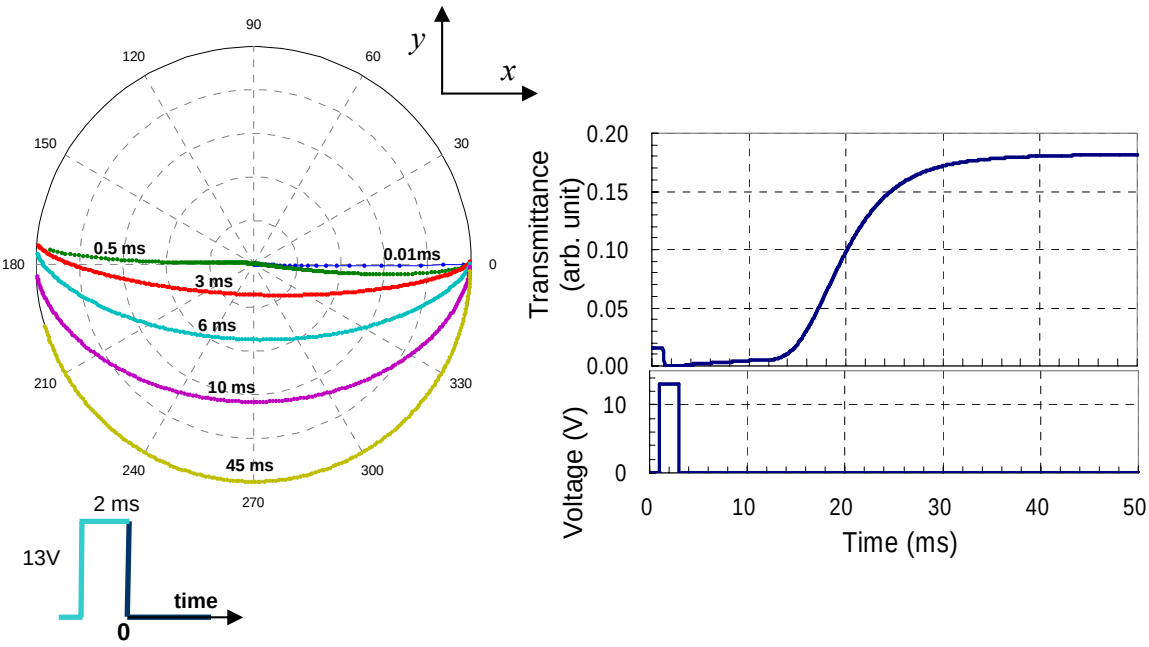

Figure 4.2 The dynamic trajectories of the directors in the normal-twisted relaxation process (a) and the optical response (b) when the cell was switched form U state to T state by applying a 2 ms pulse of 13V.

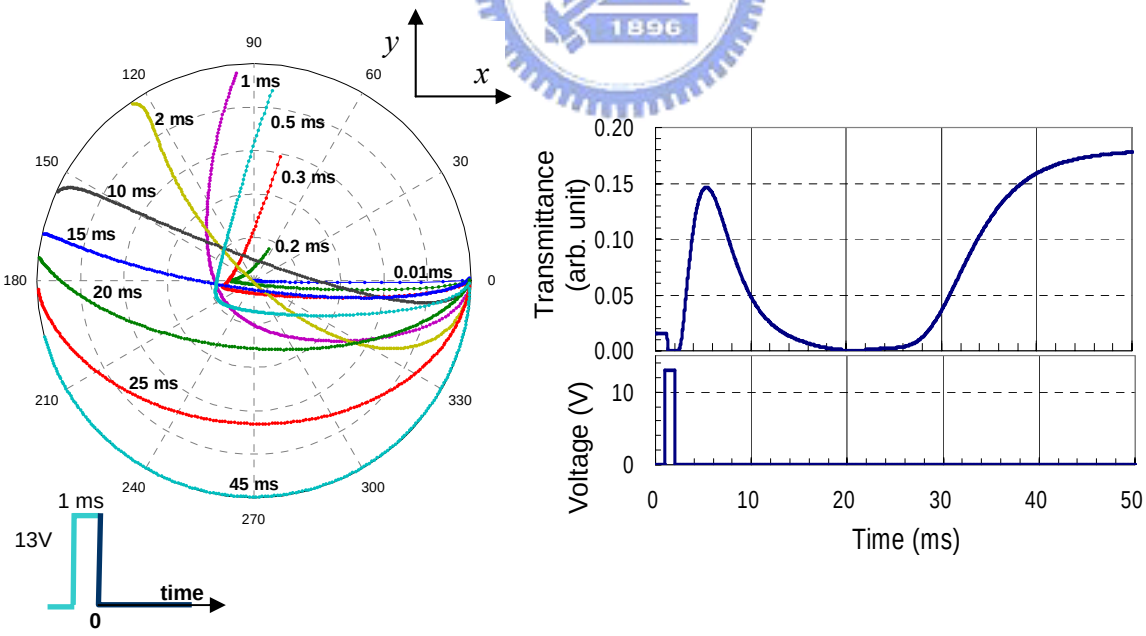

Figure 4.3 The dynamic trajectories of the directors in the over-twisted relaxation process (a) and the optical response (b) when the cell was switched form U state to T state by applying a 1 ms pulse of 13V.

At the end of the 2 ms pulse in Figure 4.4(a), $\vec{n}_b$ has already reached a balance while

α_b (black line) is almost 90°. This situation resembles the anchoring energy breaking that Dozov has proposed. When the field suddenly vanishes, the tilt angles of the directors around the middle layers become larger than 90° due to the backflow effect. [8,9] However, according to Eq. (4-2), the polar anchoring torque acting on $\vec{n}_b$ is nearly zero, because α_b is almost 90°. Mainly due to the backflow effect, $\vec{n}_b$ is directed toward the $-x$ direction. This behavior of $\vec{n}_b$ is explicitly shown as ϕ_b (gray line) jumps from 0° to 180° while α_b decreases gradually in Figure 4.4(a). As a whole, the directors of the cell spread as the directors tilt down and relax to the T state as shown in Figure 4.2(a). This normal-twisted relaxation process agrees well with the model that Dozov has proposed.

However, at the end of a 1 ms pulse as shown in Figure 4.4(b), $\vec{n}_b$ is nearly vertical, but α_b has not yet reached 90°. For the same reason as the 2 ms pulse, the tilt angles of the directors around the middle layers are getting larger than 90°. However, because α_b is slightly smaller then 90°, the polar anchoring torque is larger than that of the normal-twisted relaxation process and tends to make $\vec{n}_b$ tilt downwards in the $+x$ direction. On the other hand, the azimuthal anchoring, which is nearly one-tenth of the polar anchoring, allows $\vec{n}_b$ to move easily in the azmuthal direction. Therefore, the combination of the surface anchoring torque, the elastic torque and the shear viscosity torque makes α_b decrease and ϕ_b increase slowly as shown in Figure 4.4(b). As a whole, the cell takes the over-twisted process as shown in Figure 4.3(a) and slowly relaxes to the T state. Due to the slow swing of ϕ_b, the relaxation time of the over-twisted relaxation process is longer than that of to the normal-twisted relaxation process.

When we further reduce the duration of the 13 V pulse to 0.5 ms, $\vec{n}_b$ is far from vertical at the end of the pulse as shown in Figure 4.4(c). Since ϕ_b is always around the $+x$ direction, the cell returns to the U state. However, if we increase the voltage of the 0.5 ms pulse, the directors are pulled faster. When $\vec{n}_b$ reached the vertical within the pulse duration, the cell can be switched to the T state. The threshold voltage, which is defined as the minimum voltage needed to change the cell from the U state to the T state, becomes larger when we reduce the pulse duration. This relationship agrees quite well with the experiments performed by Giocondo *et al*. in Figure 3 of reference 10.

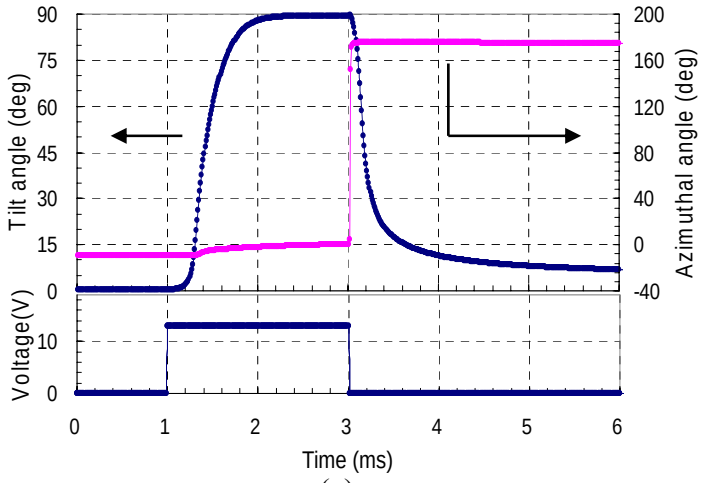

(a)

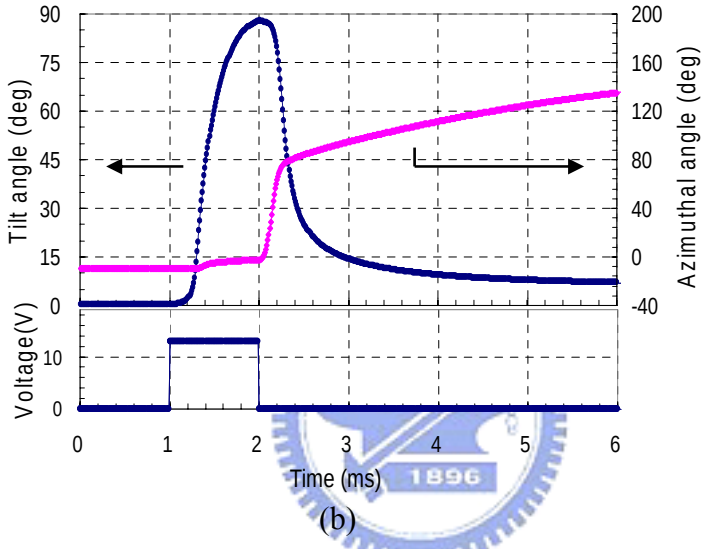

(b)

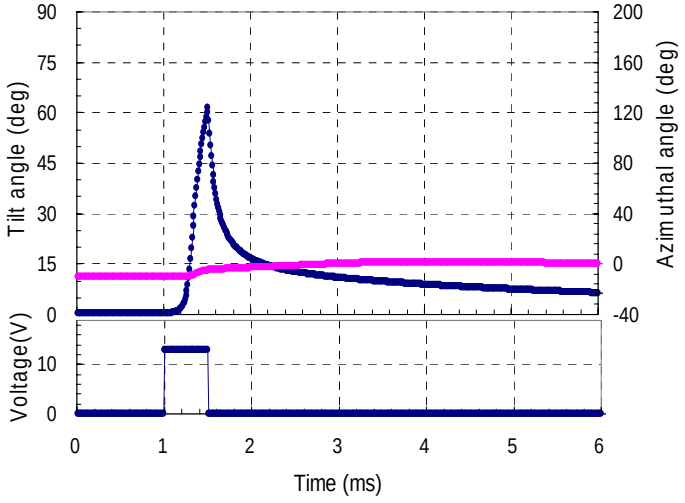

(c)

Figure 4.4 The dynamic tilt and azimuthal angles of $\vec{n}_b$ when we applying pulses of 13V with different duration: (a) 2 ms (b) 1 ms and (c) 0.5 ms. The tilt and azimuthal angles of $\vec{n}_b$ in the normal-twisted relaxation process and the over-twisted relaxation process are shown in (a) and (b), respectively. When the pulse is too short which is the case of (c), the cell is not switched to the T state and relaxes to the U state.

Through the analysis, we have distinguished the normal-twisted and over-twisted relaxation processes when the cell is switched to the T state by 2 ms and 1 ms pulses, respectively. Moreover, if the pulse is too short, the cell cannot be switched to the T state and returns to the U state. In fact, these phenomena exist in a broad range of *d/p* (cell thickness *d* over the chiral pitch *p*) in the simulation. For *d/p* = 0.25, the two stable states have the same elastic free energy density. However, in the experiments, to switch the cell from the U state to the T state is easier than to switch it from the T state to the U state with *d/p* = 0.25. It is easier for the cells switched from the T state to the U state with a smaller *d/p.* In order to make the switch equally easy, we chose *d/p* to be smaller than 0.25 in our simulation. Even with *d/p* = 0.25, by applying different duration pulses we still obtain normal-twisted and over-twisted relaxation processes when the cell is switched from U state. If the pulse is too short, the cell remains at the U state.

This study enables us to understand the transient behavior of the directors when applying a pulse. From the results of the simulation, we may optimize the pulse duration and the voltage to achieve a fast relaxation time.

4.4 Relation between polar anchoring energy coefficients and voltage of the switching pulses

In this section, we focus on the relationship between the polar anchoring coefficient of the bottom boundary and the voltage required to switch the cell from the U state to the T state. We confine the pulse duration to 1 ms and applied it to a 1.5μm thickness LC cell in order to make the surface directors reach balance within the pulse duration. We obtain the minimum required voltage as a function of the polar anchoring energy coefficient by simulation with the same LC material used in last section and the cell parameters shown in Table 4-II. The simulated curve is shown as the line A in Figure 4.5 with a series of blue triangles. For a cell with the anchoring energy properties are fixed, the pulses with higher applied voltage (the upper part of the diagram) can be used to switch the cell to the T state and with the lower voltages make the cell remain in the U state. From last section, we know that if the pulse duration of the applied pulse gets shorter, the minimum required voltages are higher and the line A will shift to the left. However, if the duration becomes longer, the line A will not move because the surface directors have already been balanced within the pulse duration.

Table 4-II The cell parameters used in the simulation.

Cell gap	1.5 μm	Pitch	8 μm
Wavelength	550 nm		
Top boundary :		Bottom boundary :	
Pretilt angle	5°	Pretilt angle	0.1°
$W_{\theta t}$,$W_{\phi t}$	1.3× 10^{-3} J/m^2	$W_{\theta b} = W_{\phi b}$	

We can roughly derive the curve without simulation by using the concept of 'anchoring breaking'. This concept is proposed by Dozov in which they only considered the movement of the surface director in the polar direction. When an electric field is applied to the cell, the surface directors begin to tilt up. When the electric field is equal to the critical field, the surface directors become completely homeotropic. The critical field is defined by the surface extrapolation length, $L = k/W_\theta$, to be equal to the electric field coherence length, $\xi = \sqrt{k/\varepsilon_0 \Delta\varepsilon}\,/E$, where k is the Frank elastic constant. For the LC thickness of d, the critical voltage can be derived as:

$$V_{critical} = E_{critical} \cdot d = \frac{dW_\theta}{\sqrt{\varepsilon_0 \Delta\varepsilon\, k}}. \tag{4-3}$$

The calculated critical voltages are plotted as the line B in Figure 4.5 with green squares. The anchoring is 'breaking' when the cell is applied above the critical voltage since the surface directors are vertical. Under this situation, the surface directors can go toward two different directions; result in the different final states. Carefully eliminate the shear flow effect will make the cell toward U state. A little shear flow will make the cell toward the T state. However, in the reality the surface directors need not to be homeotropic to be switched to the T state. Even with a little tilt from homeotropic, due to the help of the shear flow, the surface directors can be kick over and the cell can be switched to T state. Therefore, our minimum required voltage of 1 ms pulse from simulation is smaller than the critical voltage. As the voltage of the applied pulse decrease, the tilt angle of the surface director is getting smaller and the induced shear flow become smaller, the cell may remain in the U state.

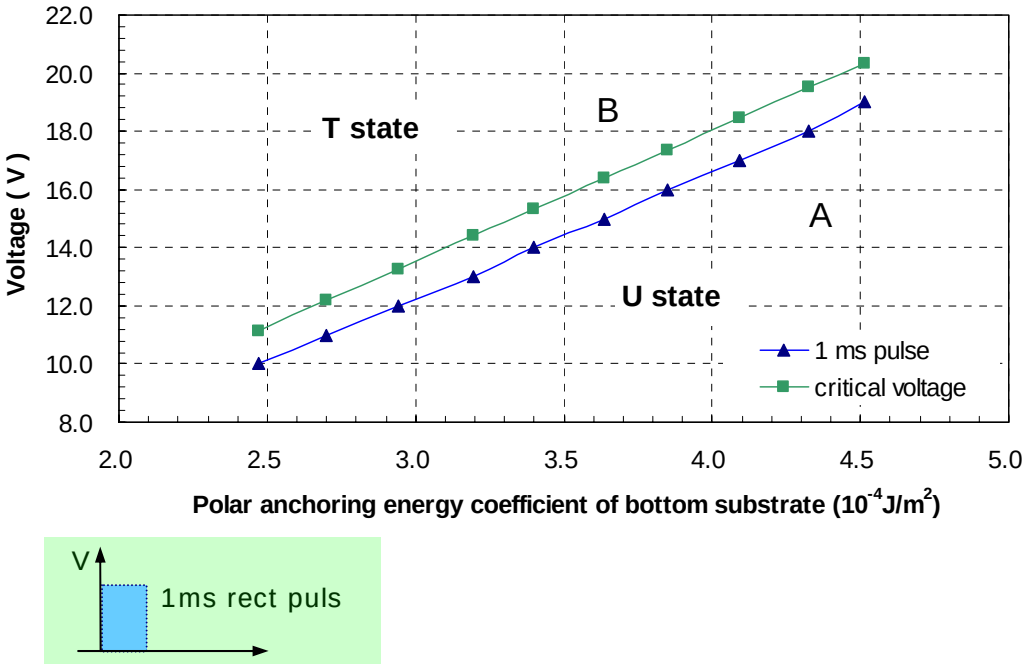

Figure 4.5 The critical voltage (square) and the minimum required voltage (triangle) as function of the polar anchoring energy coefficient for switching the cell from the U state to the T state. The pulses with higher applied voltages can be used to switch the cell to the T state and with the lower voltages make the cell remain in the U state.

In addition to the simulation with 1 ms pulse, we used a waveform of one 1 ms reset pulse followed by on 1 ms selective pulse to control the cell switched to either T state or U state. The reset pulse is used to make the surface director 'forget' where it comes from and the selective pulse makes the cell goes to the selected state. If the original state is U state, the voltage of the reset pulse should be in the upper part of line A in Figure 4.5. The existence of the selective pulse is to make the cell remain in the U state. Therefore, the voltage of the selective pulse should be in the right part of line A. To make the shear flow induced by the step between the reset pulse and the selective pulse, we choose the voltage of the selective pulse to be 1 volt less than that of the reset pulse. The maximum voltages of the reset pulse for keeping the cell in the U state are plotted as the line C with the orange squares in Figure 4.6. The reset pulse with higher voltage of line C can switch the cell to the T state and with lower voltage of that make the cell remained in the U state.

The line A of Figure 4.5 is re-plotted in Figure 4.6 for comparison. For example, if the polar anchoring energy of the bottom substrate ($W_{\theta b}$) is 1.3×10^{-4} J/m^2, we can choose the reset pulse to be 14.4 V and the selective pulse to be 13.4 V. Applying the reset pulse

only, the cell goes to the T state since it is in the upper part of line A. If the reset pulse is followed by the selective pulse, the cell goes to the U state because it is in the lower part of line C.

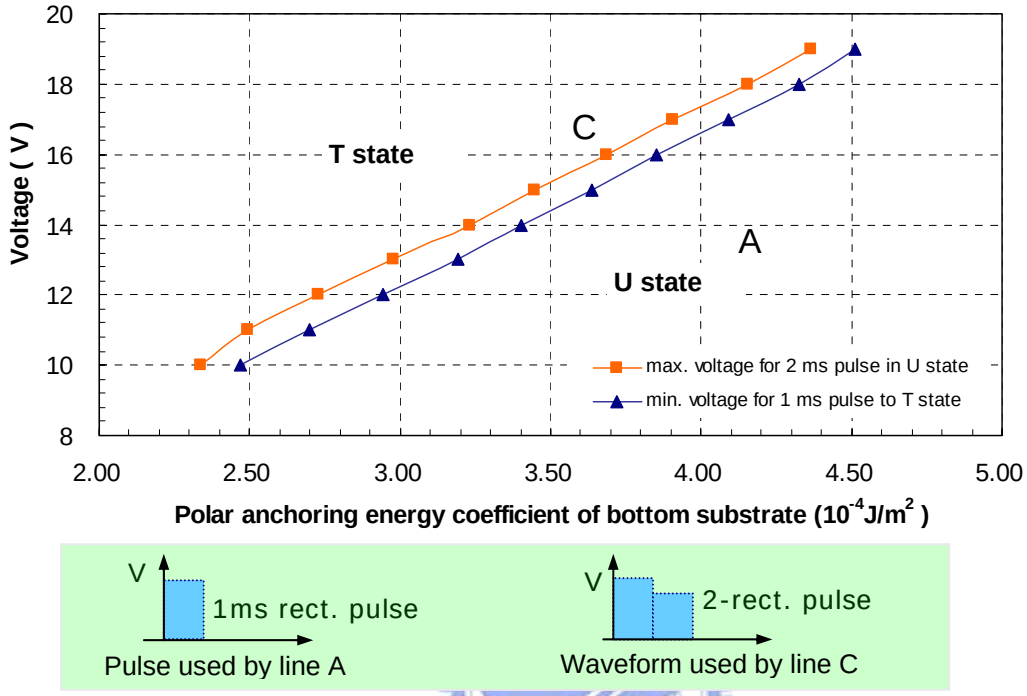

Figure 4.6 The minimum required voltage as function of the polar anchoring energy coefficient for switching the cell from the U state to the T state by using a 1ms pulse (triangle) and the 2 ms pulse (square). The pulses with higher applied voltages can be used to switch the cell to the T state and with the lower voltages make the cell remain in the U state.

Since the range between A and C lines are not very wide with the waveform we used in the simulation. The switching result is sensitive to the voltage of the pulse and $W_{\theta b}$. If $W_{\theta b}$ of the cell changes, e.g. aging, the switching result will be different from the original design. Therefore, to optimize the waveform is necessary for making BiNem device a high quality LCD.

References of Chapter 4

[1] D. W. Berreman and W. R. Heffner, J. Appl. Phys. **52**, 3032, (1981).

[2] Tie-Zheng Qian, Zhi-Liang Xie, Hoi-Sing Kwok, and Ping Sheng, Appl. Phys. Lett., **71**, 596, (1997).

[3] I. Dozov, M. Nobili, and G. Durand, Appl. Phys. Lett., **70**, 1179, (1997).

[4] I. Dozov and G. Durand, Liquid Crystals Today, **8**, 2, (1998).

[5] S. Saito, T. Takahashi, T. Chiba, and S. Tsuchida, Jpn. J. Appl. Phys. **41**, 3841, (2002).

[6] T. Takahashi, S. Tsuchida, M. Udagawa, and S. Saito, Jpn. J. Appl. Phys., **43** 1469, (2004).

[7] *DIMOS User's Guide*, vision 1.6, autronic-MELCHERS GmbH and private communications.

[8] Chih-Yung Hsieh and Shu-Hsia Chen, Appl. Phys. Lett., **83**, 1110, (2003).

[9] Shu-Hsia Chen and Chiu-Lien Yang, Appl. Phys. Lett. **80**, 3721, (2002).

[10] M. Giocondo, I. Lelidis, I. Dozov, and G. Durand, Eur. Phys. J. AP **5**, 227, (1999).

Chapter 5

Bistable chiral-tilted homeotropic nematic (BHN) liquid crystal cell

In this chapter, we proposed a new bistable mode, namely, the bistable chiral tilted-homeotropic nematic cell. The two stable states are the tilted homeotropic state and the twisted state. The switching mechanisms are achieved by the backflow effect together with the anisotropic properties of the dual-frequency liquid crystal material. The experimental results of this bistable cell and the simulations are given.

5.1 Introduction

Bistable liquid crystal (LC) displays have received considerable attention recently because the power consumption can be reduced by their two (or more) stable states. Among them, the bistable twisted nematic (BTN) LC cell[1,2] (2π-BTN) can be switched between the ($\phi - \pi$) and ($\phi + \pi$) twisted states by controlling the flow effect. However, the lifetimes of these states are not very long because a more stable intermediate ϕ state exists. Although Wang and Bos[3] have achieved a long-term bistability by using multidimensional alignment structure to prevent the nucleation, the application is still limited. To make the states truly stable, several bistable modes have been demonstrated. For switching between the twisted states which differ by π, Bistable Nematic device[4] (BiNem) and comb-on-plate BTN[5] (COP-BTN) are comprised of asymmetric substrates with different anchoring energy to achieve anchoring energy breaking, and bistable chiral-splay nematic LC device (SCBN-LC) [6] and COP-BTN are constructed with three-terminal electrode structure to

produce horizontal and vertical fields. Moreover, the substrates of the Zenithal Bistabile Display[7] (ZBD) are made of the microstructure relief grating with short pitch and deep profile, and those of the micro-patterned surface alignment device[8] are patterned by using the atomic force microscope nano-rubbing technique. Due to the sophisticated substrates used in these modes, the manufacturing processes do not match the standard procedure in a typical LC display factory. On the other hand, our group has proposed the bistable chiral quasi-homeotropic[9,10] device (BCQH) in which the conventional rubbing technique is employed to align the liquid crystal molecules. However, its two stable states exist only under an electric field. This drawback hinders the desired achievement in saving energy.

In the next section, we demonstrate a new scheme of a bistable LC cell, called the bistable chiral tilted-homeotropic nematic LC (BHN) device. This device can be switched easily between the tiltedly homeotropic state (TH state) and the twisted state (T state) because of the use of dual-frequency LC material. In comparison with the above-mentioned complex treatments of substrates, we simply exploit the conventional rubbing technique, which is part of a very popular manufacturing procedure performed in LC display factories, for the treatment of substrates. In addition, the two bistable states exist without electric field. In our experiment, the external voltage we applied to switch between the two stable states was 5 V_{rms}, which is much lower than most of the bistable devices reported in the literature. Furthermore, the simulation suggests that the contrast ratios of the transmissive or reflective cells under the crossed-polarizer condition are very high, comparable to those of chiral homeotropic liquid crystal cells.[11,12]

5.2 Theory

Consider a cell with a thickness-to-pitch ratio (d/p) around one. We obtain two stable states with the pretilt angle, measured from the substrates, in a suitable range which is determined by the LC parameters and the anchoring energy of the substrates. Fig 5.1 illustrates the textures of these two states and the transition processes of the proposed bistable cell consisting of a dual-frequency liquid crystal. When the cell is in the T state, an electric field with frequency f_1 applied in the vertical direction will pull the LC molecules vertically since the liquid crystals possesses a positive dielectric anisotropy ($\Delta\varepsilon$) at the very frequency. When the molecules reach balance, the cell exhibits the biased homeotropic (BH) state. The LC molecules in BH state are balanced by the elastic deformation torque

and the electric torque. The middle-layer directors are vertical and the directors near the boundaries are slightly tilted in the rubbing direction. Once the voltage is off, the molecules relax to the tiltedly homeotropic (TH) state. The molecules in TH state are aligned nearly homogeneous with a very high tilt angle.

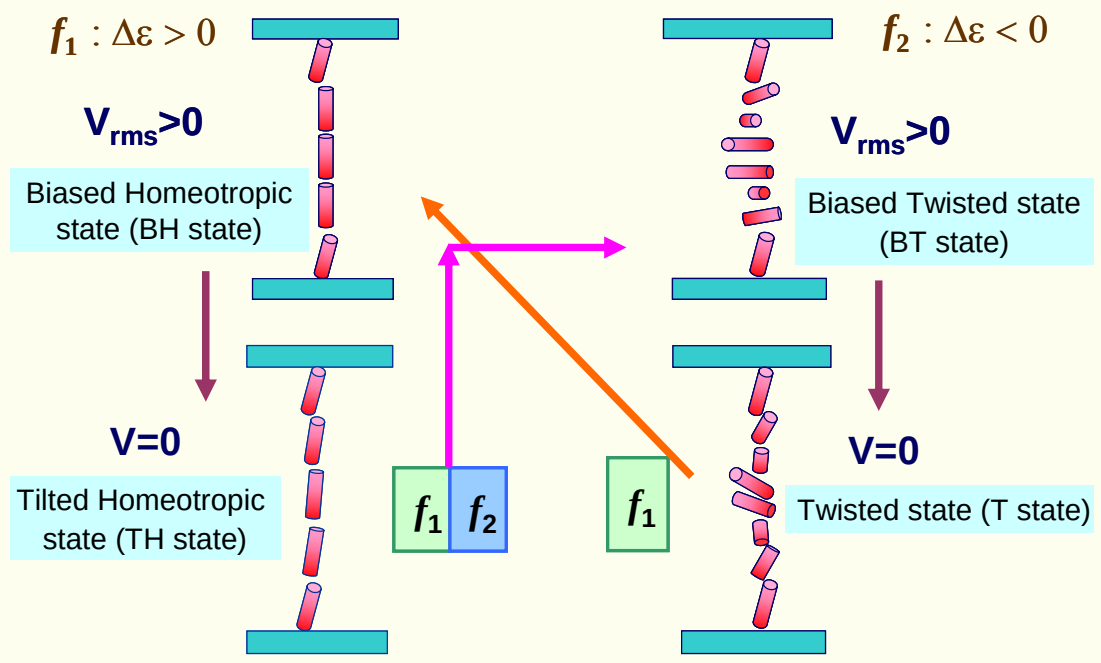

Figure 5.1 Bistable textures and transition processes of the BHN device.

To switch the TH state to T state, one can apply a pulse with frequency f_1, followed immediately by another pulse with a higher frequency of f_2. Upon the application of the first pulse, the cell is first switched to the BH state. When the frequency of the electric field is changed from f_1 to f_2, the dielectric anisotropy of the dual-frequency liquid crystal is changed to negative and the electric torque tends to align the molecules horizontally. This torque makes the directors near the substrates rotate faster than the mid-layer directors do and produces a flow velocity due to the coupling via viscous interaction The spatial variation of the velocity gives rise to the tilt angle of the middle-layer directors to be larger than $\pi/2$. This phenomenon is usually called the backflow effect. As a result, the directors of the cell rotate nearly 2π in the azimuthal angle. Finally the mid-layer directors become parallel to the substrates and the biased twisted (BT) state is generated. The directors relax to the T state with a slight tilt in the middle layer when the voltage is off.

5.3 Experimental results

To demonstrate the BCTHN device, we used indium–tin-oxide (ITO) glasses as the substrates and coated them with RN-1338 (Nissan Chemicals Co.) to form the tiltedly homeotropic alignment layers. The rubbing directions of the top and the bottom alignment layers were anti-parallel. The dual-frequency LC material we used was MLC-2048 (Merck Co.) with $\Delta\varepsilon = 3.22$ at 1 kHz and $\Delta\varepsilon = -3.4$ at 100 kHz. Pairs of the substrates were combined by using 9.9-μm spacers mixed in the adhesive to form empty cells, which were then filled with MLC-2048 with a pitch of −10 μm. The TH state and T state coexisted when the cell was first assembled. And a dark state appeared after we applied *a* 1-kHz pulse under the crossed-polarizer condition. It is quite easy to have either one of the bistable states by using the switching mechanism proposed in Figure 5.1.

The optical properties were measured under the crossed-polarizer condition with the transmission axis of the linear polarizer and the rubbing directions parallel to the *x*-axis. The light source was a He–Ne laser with a wavelength of 632.8 nm. If the cell is in the TH state or BH state, the light goes through the cell with little phase-retardation so that the appearance of the cell is dark and the transmittance low. In contrast, if the cell is in the T state or BT state, the light leaks through the second polarizer so the transmittance is higher.

Figure 5.2 shows the transient transmittance of the BCTHN cell from T state to TH state by applying a pulse (voltage = 5 V, frequency = 1 kHz). The liquid crystal possesses a positive dielectric anisotropic within the pulse duration. The oscillation of the transmittance is due to the change in phase-retardation when the twisted molecules (in T state) are pulled to the vertical direction. As most of the LC molecules become vertical (BH state), the cell appears dark. When the voltage is turned off, the LC molecules relax to the TH state of which the transmittance is also very low.

Figure 5.3 shows the transmittance from TH state to T state as well as the corresponding driving waveform. When a voltage of 5 V pulse with frequency of 1 kHz is applied to the cell, the LC molecules are switched to the BH state, keeping the transmittance almost unchanged. Then the frequency is changed to 100 kHz suddenly, the LC molecules of the middle layer tilt down in the opposite direction due to the backflow effect. Finally they lie in the *–x* direction and the cell is in the BT state. Note that the oscillation of the transmittance following the onset of the frequency change is attributed to the phase-retardation change as the directors spread into the BT state. When the voltage is off, the LC molecules relax to the T state, which is the bright state.

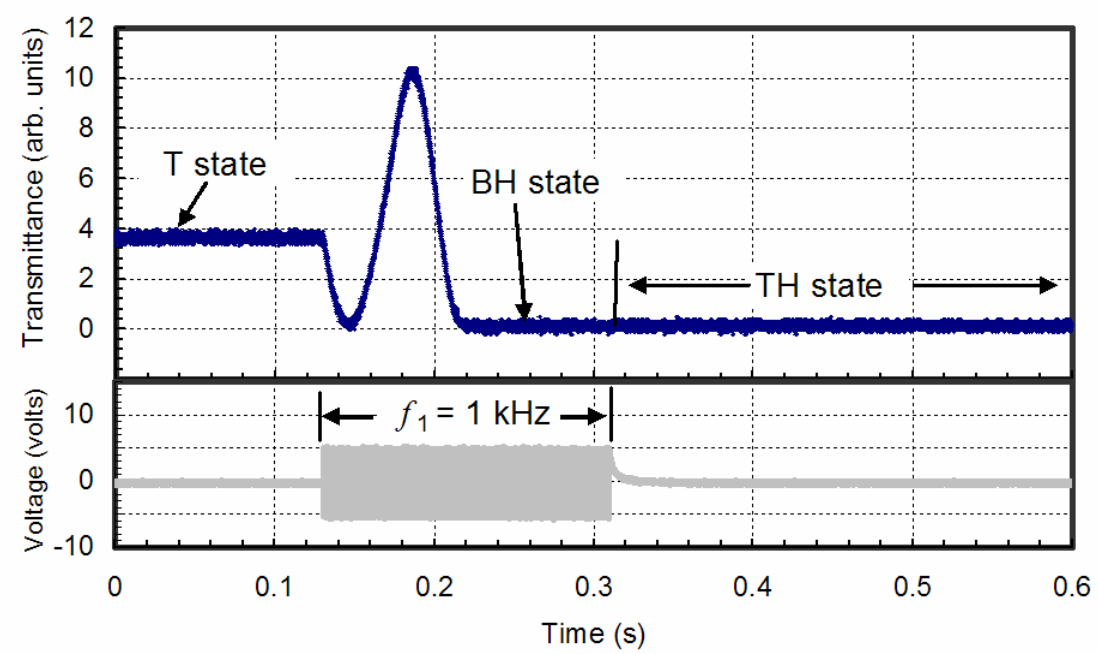

Figure 5.2 The transient transmittance and the corresponding driving waveform of the BHN device switched from the T state to the TH state. The amplitude of the driving pulse is 5 volts and the frequency is 1 kHz.

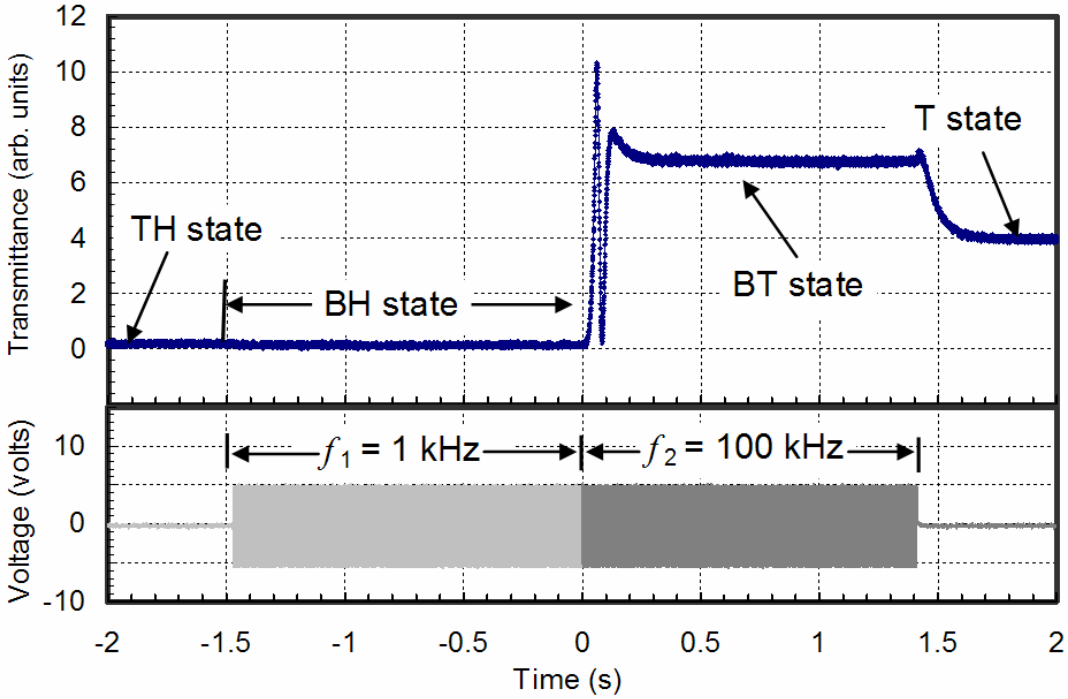

Figure 5.3 The transient transmittance and the corresponding driving waveform of the BHN device switched from the TH state to the T state. The amplitude of the driving pulse is 5 volts. The frequency is switched from 1 kHz to 100 kHz.

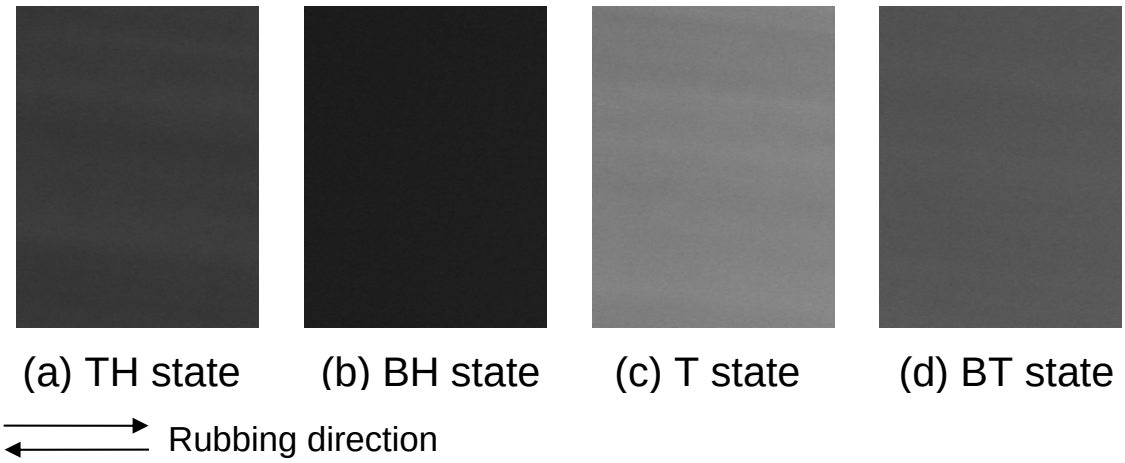

Figure 5.4 Transmission micrographs of the BHN device under the crossed-polarizer condition. (a) The tiltedly homeotropic state; (b) the biased homeotropic state; (c) the twisted state; (d) the biased twisted state.

Figure 5.4 shows the microscopic photographs of TH state, BH state, T state and BT state in the crossed-polarizer condition with rubbing directions parallel to the polarizer. The TH state is not as dark as the BH state, because most directors in the BH state are vertical while the directors in the TH state are tilted. If some misalignment of the substrates exists, the directors in the TH state form a helical structure with a small conic angle, and the transmittance of the cell increases. Since the BT state is reddish while the T state is greenish, the transmittance of the BT state is higher when using a He–Ne laser as the light source, as shown in Figure 5.2 and 5.3, and lower when taking black-and-white pictures under the microscope with a white light source. In BHN, the optimized value of $d\Delta n/\lambda$ for maximum light efficiency is related to the pretilt angle and LC parameters. In our simulations, the contrast ratio of 1000 is easily achieved at $\lambda = 550$ nm.

Experimentally, we find that the pretilt angle is crucial to the BCTHN device. As the pretilt angle is close to 90°, the cell prefers TH state and the focal conic texture[13]. However, small pretilt angle make the T state more stable. The d/p ratio is another factor to affect the bistability. A larger d/p makes the TH state absent while smaller d/p makes T state vanish. These results have been confirmed by simulation. To make this bistable device applicable, the elastic constants of the liquid crystals, which influence the free energies of the two stable states, should be optimized. Dust particles and defects on the substrates also affect the bistable states. For example, after the cell is switched to the dark state (TH state) and the whole cell appears dark for about a few minutes, some bright spots may appear slowly and extend gradually to their peripheral areas. It needs about an hour to complete this process and the final status of the cell is half TH state and half T state.

References of chapter 5:

[1] D. W., Berreman and W. R. Heffner, Appl. Phys. Lett., **52**, 3032, (1981).

[2] Tie-Zheng Qian, Zhi-Liang Xie, Hoi-Sing Kwok and Ping Sheng, Appl. Phys. Lett., **71**, 596, (1997).

[3] Bin Wang and Phillip Bos, J. Appl. Phys., **90**, 552, (2001).

[4] I. Dozov, M. Nobii, G. Durand, Appl. Phys. Lett., **70**, 1179, (1997).

[5] Fion S. Y. Yeung and H. S. Kwok, Appl. Phys. Lett., **83**, 4291, (2003).

[6] Seo Hern Lee, Kyoung-Ho Park, Tae-Hoon Yoon and Jae Chang Kim, Appl. Phys. Lett., **82**, 4215, (2003).

[7] G. P. Bryan-Brown, C. V. Brown, J. C. Jones, E. L. Wood, I. C. Sage, P. Brett and J. Rudin, SID Intl. Symp. Digest Tech. Papers, **28**, 37, (1997)

[8] Jong-Hyun Kim, Makoto Yoneya and Hiroshi Yokoyama, Appl. Phys. Lett., **83**, 3602, (2003).

[9] Li-Yi Chen and Shu-Hsia Chen, Appl. Phys. Lett., **74**, 3779, (1999).

[10] Chih-Yung Hsieh and Shu-Hsia Chen, Appl. Phys. Lett. **81**, 1110, (2003).

[11] J. S. Patel and G. B. Cohen, Appl. Phys. Lett. **68**, 3564, (1996).

[12] Shin-Tson Wu, Chiung-Sheng Wu and Kun-Wei Lin, J. Appl. Phys. **82**, 4795, (1997).

[13] W. Greubel, Appl. Phys. Lett., **25**, 5, (1974).

Chapter 6 Summery and future scope

Conventionally, the boundary directors are assumed to be rigidly anchored on the alignment layer. In this dissertation, we consider the non-rigid boundary condition and investigate the boundary parameters: the pretilt angle and the anchoring energy density. In the study of the pretilt angle, we proposed a method to determine the pretilt angle of the reflective LCD. And in the study of the anchoring energy density, we found the higher orders term of the anchoring energy density should not be neglected when the applied field is large. We also investigate the effect of the anchoring energy coefficient on the flow effect through BiNem cell, which use one weak and one strong alignment layers. Different dynamic behaviors are observed when we apply the pulses of 13 V with different durations to a U state cell. One, which is the relaxation process of the 2 ms pulse, agrees well with the model proposed by Dozov and we call it the normal-twisted relaxation process. The other is similar to the results simulated by Takahashi and we call it the over-twisted relaxation process. Moreover, the relaxation time of the over-twisted relaxation process is 1.5 times of the normal-twisted relaxation process. If we further reduce the duration of the pulse to 0.5 ms, the cell is unable to be switched to the T state. The mechanisms of the different behaviors are explicitly explained through the tilt and azimuthal angles of the director on the weak anchoring boundary in the dynamic process.

Moreover, we propose and we demonstrate a new scheme of a bistable LC cell, called the bistable chiral tilted-homeotropic nematic LC (BHN) device. This device can be switched easily between the tiltedly homeotropic state (TH state) and the twisted state (T state) because of the use of dual-frequency LC material and the shear flow effect. Comparing to the complex treatments of substrates, we simply exploit the conventional rubbing technique, which is part of a very popular manufacturing procedure performed in LC display factories, for the treatment of substrates. In addition, the two bistable states

exist without electric field. In our experiment, the switching voltage we applied was 5 V, which is much lower than most of the bistable devices reported in the literature.

There are a lot of studies on the cell with the boundary directors closed to homeotropic and homogeneous alignment. Most of these studies are restricted to the rigid boundary condition. Therefore, there are a broad range of the boundary conditions, including the hard to the weak anchoring conditions, which have not been investigated. Combining with the various anchoring condition and the flow effect, there may exist some other bistable modes. Moreover, the flow effect of the patterned electrodes, e.g. IPS and FFS, has seldom been studied. The effects of the anchoring properties of these alignment layers on the flow effect will be worth investigation.

Vita

姓名：徐芝珊

住址：苗栗縣竹南鎮大厝里 9 鄰大厝 56 號

生日：民國五十一年十二月三十一日

學歷：國立交通大學電子物理系　　民國七十三年六月

國立交通大學光電工程研究所　　民國七十五年六月

經歷：國立交通大學電信工程系講師　　民國七十六年八月～民國七十六年六月

國立彰化師範大學物理系助理　　民國八十八年八月～民國八十九年七月

國立彰化師範大學科教所助理　　民國八十九年八月～民國九十年三月

已發表著作：

Journal papers

1. Jy-shan Hsu, Bau-Jy Liang and Shu-Hsia Chen, "**Bistable chiral tilted-homeotropic nematic liquid crystal cells**", Appl. Phys. Lett., 85, 5511, 2004.
2. Jy-shan Hsu, Bau-Jy Liang and Shu-Hsia Chen, "**A simple method for determining the pretilt angle of a vertically aligned reflective LCD**", IEEE Transaction on Electron Devices, vol.52, no.5, p.918, 2005.
3. Shu-Chan Hsiao, Jy-shan Hsu, Bau-Jy Liang and Shu-Hsia Chen, "**Cell-gap and pretilt-angle determination of a vertically aligned reflective liquid-crystal display**", Journal of SID, vol.11, no.4, p.629, 2003.
4. Jy-shan Hsu, Bau-Jy Liang and Shu-Hsia Chen, "**Transient Behaviors of the bistable nematic liquid crystal cells"**, Jpn. J. Appl. Phys (in press).
5. Jy-shan Hsu, Mei-Chi Hsieh, Chia-Leng Yang, Bau-Jy Liang and Shu-Hsia Chen, "**A Method to Determine the Higher Order Polar Anchoring Coefficients for the Non-Twisted Liquid Crystal Cells"**, Jpn. J. Appl. Phys (in press).

Conference papers：

1. Jy-Shan Hsu, Chia-Leng Yang, Mei-Chi Hsieh, Bau-Jy Liang and Shu-Hsia Chen, "**The Influence of the Alignment Layers to the Achoring Energy of Non-twisted Liquid Crystal Cells**", 中國液態晶體學 2004 年年會暨研討會論文集, 台北科技大學, p70, 2004.
2. Ting-Yi Wu, Jy-shan Hsu, Shu-Hsia Chen, "**Pretilt angle measurement for the non-twisted nematic liquid crystal cell**", 2004 Taiwan Display Conference, pp. 191, 2004.
3. Jy-shan Hsu, Bau-Jy Liang, Shu-Hsia Chen, "**Study on the Transient Behaviors in Bi-stable Nematic Liquid Crystal Cells**", 2003 中國液態晶體研討會, pp. 56, 2003.
4. Hui-Wen Yang, Jy-shan Hsu, Shu-Hsia Chen, Jung Y. Huang, Bau-Jy Liang, "**An Improved Method for Measuring Azimuthal Anchoring Energy**", International Display Manufacturing Conference & FPD Expo, Taipei Int'l Convention Center, pp. 595, 2003
5. Hui-Wen Yang, Jy-shan Hsu, Shu-Hsia Chen, Jung Y. Huang, Bau-Jy Liang, "**An improved method for simultaneous measurement of twist angle and cell thickness in TN cell**", 2002 台灣光電科技研討會, pp. 10, 2002.
6. Bau-Jy Liang, Jy-shan Hsu, Shu-Hsia Chen, "**Comparing on the color-shift of Conic CCLCD with others 4-domain liquid crystal Displays**", 2001 中國液態晶體研討會, pp.74, 2002.

專利：

1. 徐芝珊、梁寶芝、王淑霞、劉錦璋，一種雙穩態液晶顯示裝置及其驅動方式，申請中華民國專利、美國專利中、日本專利及大陸專利。